nature reviews materials

https://doi.org/10.1038/s41578-026-00893-8

Review article

Check for updates

Many-body entanglement in solid-state emitters

Emma Daggett[1], Christian M. Lange[2], Bennet Windt[3,4], Arshag Danageozian[5,6], Alexander Senichev[7,8], Jordi Arnau Montañà-López[3,4], Chanchal[1], Kinjol Barua[1,7], Xingyu Gao[2], Zhaoyun Zheng[9], Vijin Kizhake Veetil[10], Souvik Biswas[11], Jonas M. Peterson[1], Na Liu[1], Chuchuan Hong[9], Teri Odom[9], Matthew Pelton[10], Tongcang Li[2,7], Jelena Vučković[11], Vladamir M. Shalaev[7,8], Alexandra Boltasseva[7,8], Sophia E. Economou[5,6], Jonathan D. Hood[1,2], Valentin Walther[1,2], Rahul Trivedi[3,4] & Libai Huang[1,7] ✉

Abstract

The preparation and control of quantum states lie at the heart of quantum information science. Recent advances in solid-state quantum emitters (QEs) and nanophotonics have transformed the landscape of quantum photonic technologies, enabling scalable generation of quantum states of light and matter. A new frontier in solid-state quantum photonics is the engineering of many-body interactions between QEs and photons to achieve robust coherence and controllable many-body entanglement. These entangled states, including photonic graph and cluster states, superradiant emission and emergent quantum phases, are promising for quantum computation, sensing and simulation. However, intrinsic inhomogeneities and decoherence in solid-state platforms pose considerable challenges in realizing such complex entangled states. This Review provides an overview of fundamental many-body interactions and dynamics at the light–matter interfaces of solid-state QEs and discusses recent advances in mitigating decoherence and harnessing robust many-body coherence.

Sections

[1]Department of Chemistry, Purdue University, West Lafayette, IN, USA. [2]Department of Physics and Astronomy, Purdue University, West Lafayette, IN, USA. [3]Max Planck Institute of Quantum Optics, Garching, Germany. [4]Munich Center for Quantum Science and Technology, Munich, Germany. [5]Department of Physics, Virginia Tech, Blacksburg, VA, USA. [6]Virginia Tech Center for Quantum Information Science and Engineering, Blacksburg, VA, USA. [7]Elmore Family School of Electrical and Computer Engineering, Purdue University, West Lafayette, IN, USA. [8]Birck Nanotechnology Center, Purdue University, West Lafayette, IN, USA. [9]Department of Chemistry, Northwestern University, Evanston, IL, USA. [10]Department of Physics, University of Maryland, Baltimore County, Baltimore, MD, USA. [11]Department of Electrical Engineering, Stanford University, Stanford, CA, USA. ✉e-mail: libai-huang@purdue.edu

Introduction

Harnessing the power of quantum information science now depends on building entanglement between many quantum bits (qubits) while maintaining their coherence[1]. Despite exquisite control of individual qubits, the field faces a critical challenge: generating robust and efficient many-body entanglement at scale. Although many foundational demonstrations of quantum information have focused on atoms and ions, solid-state platforms offer distinct advantages for scaling to many qubits through their ability to be miniaturized and integrated on-chip[2]. Beyond scalability, solid-state quantum emitters (QEs) offer novel functionality, for example large dipole moments, strong nonlinear interactions or accessible spin registers. Such enhanced interactions open up new regimes of correlated dynamics, aiding the creation of large-scale entangled states. Moreover, solid-state platforms have natural compatibility with integrated photonics, enabling a full suite of on-chip capabilities such as optical manipulation, photon detection and electronic control (Fig. 1, left). By tailoring the interactions of solid-state QEs — whether through photonic modes or direct dipole–dipole coupling in hybrid light–matter systems — one can generate a wide range of many-body entangled states[3–9]. These include metrological states in which signal-to-noise ratio scales with photon number N rather than the classical $\sqrt{N}$ limit, cluster states for measurement-based quantum computation, and states with built-in error correction or resilience to photon loss for entanglement distribution (Fig. 1, right). Looking forward, solid-state platforms with tunable interactions will allow the exploration of new classes of photonic states that could transform the practicality of quantum photonic technologies.

Important advances have been made in both solid-state QEs and nanophotonics (Fig. 1). Various solid-state systems, including colour centres in wide-bandgap materials, epitaxial and colloidal quantum dots (QDs), molecules and 2D materials, have been harnessed as QEs[10–23]. In parallel, advancements in nanophotonics have enabled the production and manipulation of light on a chip[24–30]. Despite these advances, achieving robust many-body entanglement in solid-state emitters remains a central challenge. This challenge arises from intrinsic inhomogeneities and dephasing in QEs, which limit the coherence required for robust and scalable entanglement, as well as from difficulties in integrating QEs with high-quality photonics. A central open question is how to engineer light–matter interactions and collective

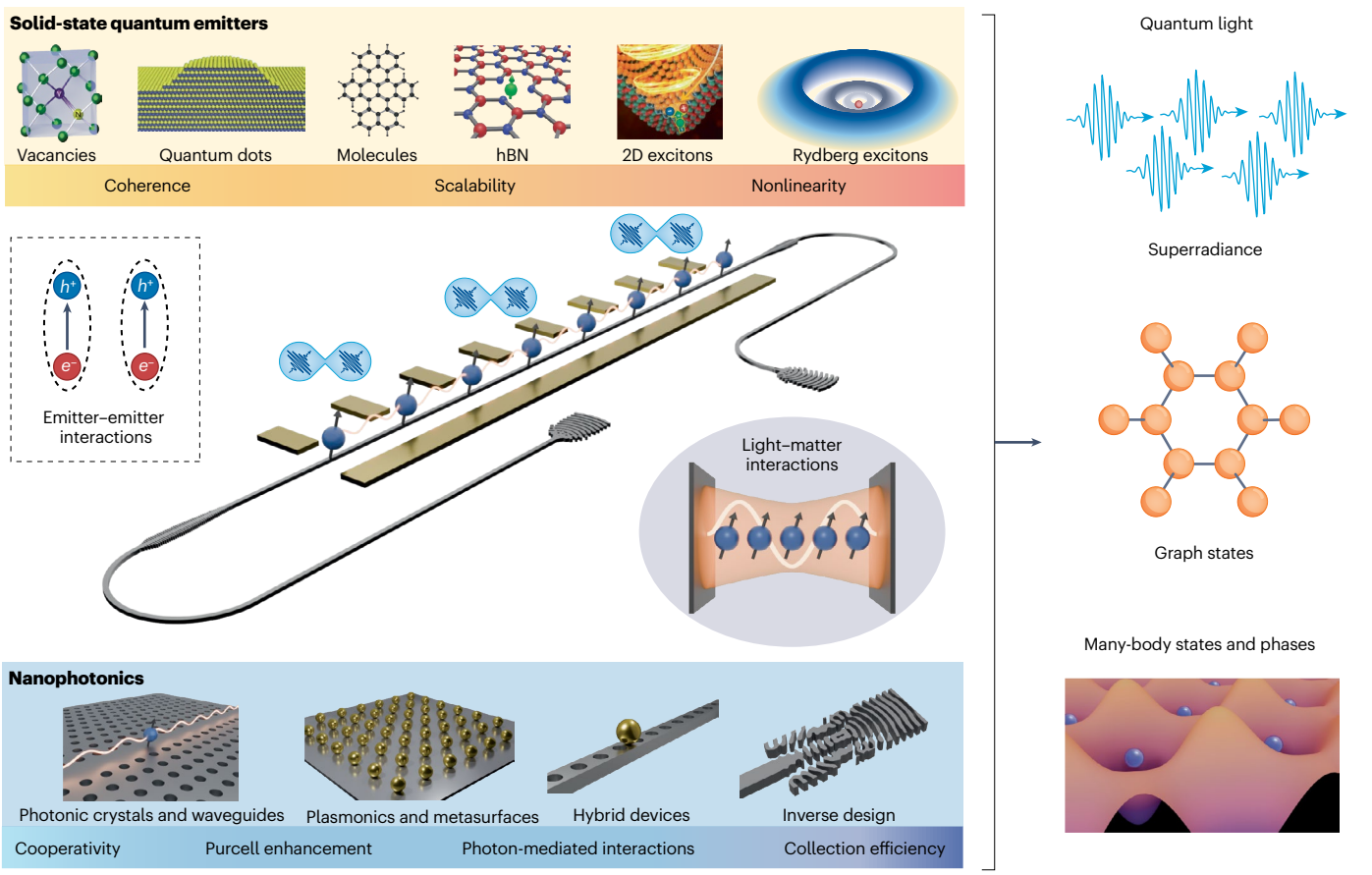

Fig. 1 | Overview of achieving many-body entanglement with solid-state quantum emitters integrated in nanophotonics. Representative quantum emitter platforms, including vacancies in wide-bandgap crystals, epitaxial quantum dots, molecules, hexagonal boron nitride (hBN) defects, 2D excitons and Rydberg excitons, categorized by their complementary strengths in properties such as coherence, scalability and intrinsic nonlinearity (top left). Photonic interfaces, which enhance light–matter coupling and mediate long-range emitter–emitter interactions through coupling to shared modes (middle left). Nanophotonic systems, including photonic crystal cavities and waveguides, plasmonic structures, hybrid devices and inverse design, that enable programmable photon-mediated couplings (bottom left). These capabilities yield quantum-optical resources (superradiance, multiphoton cluster or graph states, and quantum phase transitions) and enable interacting many-body states (right). Left panel quantum-dot image reprinted from ref. 19, Springer Nature Limited. 2D exciton image reprinted from ref. 22, Springer Nature Limited.

emitter dynamics to enable not only generation of more photons but also controllable many-body entangled states that are resilient against disorder and noise, and can thus maintain coherence over meaningful timescales.

In this Review, we focus on the emerging frontier of many-body effects in solid-state quantum photonics. Specifically, we highlight strategies for designing and controlling collective interactions, both between emitters and between photons, to realize complex quantum states such as graph and cluster states, correlated phases and superradiant emission. Emitter–emitter and light–matter interactions enable the creation of controllable entangled many-body states in a variety of systems (Fig. 1). We begin by addressing coherence and control at the single-emitter level, discussing the fundamental limits of optical and spin coherence as well as strategies for stabilization. We then examine mechanisms for realizing many-body interactions between QEs and explore how coupling to nanophotonic structures can be used to engineer, mediate and protect these interactions from decoherence. Next, we consider approaches to achieving strong photon nonlinearities and review deterministic protocols for generating complex multiphoton entangled states, such as cluster and graph states. We conclude with an outlook on applications in quantum sensing, metrology, computation and simulation, and highlight promising directions for future research.

Coherence and control at the single-emitter level

Solid-state QEs now span several distinct material platforms (Fig. 1, top), each offering complementary strengths for quantum photonic applications. Defect centres in wide-bandgap crystals, for example nitrogen–vacancy (N–V) and silicon–vacancy (Si–V) centres in diamond, silicon-vacancy (V_{Si}) centres in silicon carbide, and emitters in hexagonal boron nitride (hBN), provide stable, atom-like QEs. Epitaxially grown semiconductor QDs and their colloidal counterparts offer strong optical transitions and near-unity quantum efficiencies through bandgap engineering. Two-dimensional materials host tightly bound excitons with large oscillator strengths, enabling room-temperature operation and novel moiré-engineered interactions. Rare-earth ions embedded in crystalline hosts combine narrow optical transitions with exceptionally long-lived spin states. Organic molecules in organic matrices achieve lifetime-limited emission with high photostability. For comprehensive discussion of these various classes of solid-state QEs, readers are directed to recent specialized reviews[31–33]. A major challenge in solid-state QEs is maintaining optical and spin coherence in the presence of environmental interactions (Box 1). Phonons in the lattice, stray charges, surface effects and nuclear spins all undermine the ideal two-level character of the system.

Optical coherence

Photon indistinguishability — having identical frequency, polarization and temporal profiles — is essential for quantum interference effects: when two indistinguishable single photons arrive simultaneously at a 50:50 beamsplitter, they bosonically coalesce and exit the same port, producing a dip in two-detector coincidences, the Hong–Ou–Mandel dip. This indistinguishability enables interference both between consecutive photons from a single emitter and, critically, between photons from multiple emitters to generate entanglement. The degree of indistinguishability directly depends on the emitter's optical coherence. Photon emission arises from a cycle of excitation and emission, including radiative and non-radiative decay pathways (Box 1). The coherence of the emitted photon is fundamentally related to the optical transition linewidth, which in turn depends on both population decay time (T_1) and total dephasing time (T_2). As dephasing is typically fast in the solid state owing to interactions between the QE and its environment, a key challenge for photon indistinguishability is to achieve a much higher radiative emission rate than the dephasing rate. Near-lifetime-limited linewidths (where pure dephasing approaches zero) have been achieved in a few classes of QE systems, including Si–V centres in diamond[34,35], self-assembled QDs[36–38] and organic molecular emitters such as dibenzoterrylene (DBT)[16,39].

The zero-phonon line (ZPL) emission is typically accompanied by broad phonon sidebands at room temperature, evidencing considerable phonon coupling. For example, the N–V centre in diamond has a prominent phonon sideband (only ~3% of its emission decays into the ZPL at room temperature); the Si–V centre's inversion-symmetric structure leads to a larger Debye–Waller factor (~70% of photons decay into the ZPL at cryogenic temperatures) and reduced spectral diffusion. Optical coherence measurements of shallow Si–V centres in nanodiamonds have achieved nearly lifetime-limited linewidths of ~100 MHz (ref. 34). Epitaxial QDs typically have fast radiative rates and can also approach transform-limited emission under resonant excitation at low temperature, promising highly indistinguishable photons[40], although they remain susceptible to dephasing. In III–V QDs, for example, slow charge noise in the surrounding semiconductor produces spectral diffusion and increases the homogeneous linewidth beyond the transform limit (~160 MHz for a 1-ns radiative lifetime), degrading two-photon interference and complicating multiemitter protocols[11,41].

Two-dimensional materials such as hBN[17,42] and transition metal dichalcogenides (TMDs)[43] have attracted considerable research interest, primarily owing to their low fabrication cost, engineerable optical properties, and relative ease of integration with photonic structures[3,44,45]. However, in 2D QEs, coherence times are limited by strong coupling to phonons and susceptibility to spectral diffusion, owing to local charge fluctuations and strain fields[46]. For instance, hBN-based emitters frequently show broad linewidths (several gigahertz) at room temperature, largely attributed to phonon sidebands and to the fluctuating electrostatic environment arising from surface contaminants and intrinsic charge noise[47,48]. Homogeneous linewidths down to tens of megahertz have been achieved at cryogenic temperatures (~5 K) under resonant excitation[49], corresponding to coherence times approaching tens of nanoseconds — although substantial emitter-to-emitter variation remains. Similarly, TMD-based QEs, such as localized excitons in WS_2 or WSe_2 monolayers, typically show linewidths broadened by acoustic phonon coupling, spectral wandering and environmental fluctuations[14,50]. Consequently, achieving transform-limited lines in 2D QEs remains a central challenge in obtaining indistinguishable photons. For example, photon indistinguishability from hBN defects remains limited: an interference visibility of ~58% has been reported at 4 K (refs. 51,52), whereas near-unity indistinguishability has been demonstrated for QDs[53,54].

Coherence at the spin–photon interface

Many QEs, such as the N–V centre in diamond and the V_{Si} in silicon carbide, have an optically addressable spin degree of freedom that enables entanglement of multiple spin qubits. These experiments entail the generation of a spin–photon entangled state, followed by the detection of clicks at one detector, heralding the formation of remote spin–spin entanglement. The spin coherence time is generally much longer than the optical coherence time, but it too is limited by environmental noise. Spin dephasing is primarily due to magnetic

Box 1 | Properties of solid-state quantum emitters

Localized single-photon emitters

In an ideal two-level system, the excited-state decay rate Γ depends on frequency (ω) and dipole moment (d): $\Gamma \propto \omega^3 d^2$. However, solid-state environments introduce multiple mechanisms for deviation from this behaviour (see the figure, panel **a**).

Zero-phonon line and phonon sidebands

Coupling to lattice vibrations and other degrees of freedom partitions optical emission into distinct spectral components (see the figure, panels **a** and **b**). The zero-phonon line (ZPL) represents direct electronic transitions, whereas competing decay pathways include phonon-assisted transitions that create a redshifted phonon sideband (PSB). Molecular species may also decay into their vibrational manifold. The Debye–Waller factor quantifies the fraction of emission into the ZPL: DW = $I_{ZPL}/(I_{ZPL} + I_{PSB})$. This ranges from ~3% for nitrogen–vacancy centres to ~70% for silicon–vacancy (Si–V) centres and to >95% for epitaxial quantum dots. Low ZPL emission may be mitigated by coupling to optical cavities, where the Purcell effect can preferentially enhance decay into the ZPL.

Dephasing and spectral wandering

Lifetime-limited emission occurs when photon linewidth is determined solely by the emitter's natural lifetime: $\Delta\nu = 1/(2\pi T_1)$. In solid-state systems, interactions with the environment introduce dephasing mechanisms that cause the transition energy to fluctuate, destroying coherence and broadening spectral lines. The optical coherence time T_2 is given by $1/T_2 = 1/2T_1 + 1/T_\varphi$, where $1/T_\varphi$ is the pure dephasing time. Fast elastic phonon scattering causes homogeneous broadening (see the figure, panel **c**) that increases rapidly with temperature and can be enhanced by low orbital symmetry. Slower processes such as stochastic fluctuations, drift or random telegraph switching from charge fluctuations, and discrete charge-state conversion or shelving in dark states cause spectral diffusion and degrade long-term stability (see the figure, panel **d**).

Inhomogeneous broadening

Solid-state quantum emitters (QEs) also suffer from inhomogeneous broadening (see the figure, panel **e**) — emitter-to-emitter variations arising from strain fields, local electric fields and compositional differences that broaden ensemble spectra. Strategies to overcome inhomogeneous broadening include improved sample preparation, post-selection of spectrally matched emitters, and active tuning through electric fields or strain (see the figure, panel **f**) to achieve spectral alignment (see the figure, panel **g**).

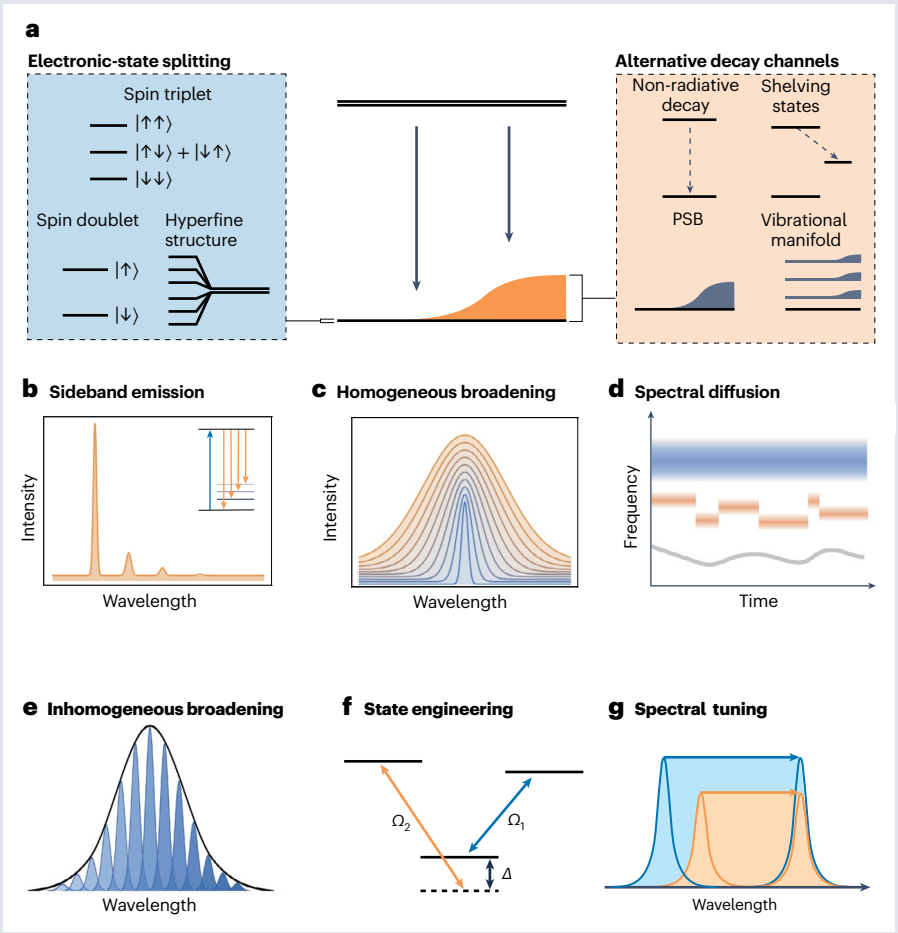

Spin coherence

Many QEs also host an optically addressable spin that can serve as a long-lived quantum memory[292,293]. The fine structure of the ground and excited-state manifolds is governed by crystal-field symmetry, spin–orbit coupling and spin–spin interactions. Spin coherence, the ability of a spin to preserve quantum phase relationships over time, is quantified by the longitudinal relaxation time ($T_{1,spin}$) and the transverse coherence time ($T_{2,spin}$) describing the persistence of the spin population and the phase coherence of the superposition states, respectively. Spin dephasing describes the degradation of this coherence, primarily due to magnetic noise from nuclear spin baths, paramagnetic impurities and spin–phonon processes. Processes such as spin–orbit coupling can dually affect spin and optical coherence.

Delocalized emitters

In addition to localized emitters, excitons in 2D transition metal dichalcogenides and other semiconductors can act as QEs whose wavefunctions extend and remain mobile over tens of nanometres to micrometres[294,295]. Although typically less coherent, their interactions are long range and can exhibit van der Waals-type or dipolar scaling depending on excitation configuration. Overlapping excitons enable collective phenomena even without precise positional control[296].

noise coupling to the emitter's spin, including interactions with nuclear and undesired electronic spin baths, spin–orbit coupling to lattice vibrations, and fluctuations in external magnetic and electric fields (Box 1). Single N–V centre electron spins can maintain coherence for a few milliseconds at room temperature[55]. This remarkable baseline is due to diamond's stiff lattice (weak spin–phonon coupling) and low nuclear spin density, and can be further extended using dynamical decoupling sequences. The Si–V centre in diamond offers a contrasting case study; its ground-state spin is strongly coupled to orbital degrees of freedom, making it sensitive to lattice vibrations[56]. At liquid-helium temperatures (~4 K), Si–V spins suffer rapid dephasing, of the order of tens of nanoseconds in natural diamond[57,58].

Discoveries of spin-active defects in hBN[17,21,59–61] have established it as a platform for spin-based quantum functionalities. However, spin coherence times (T_2^*) for these defects remain limited by hyperfine interactions with abundant nuclear spins, charge noise and lattice vibrations. Initial coherence measurements revealed very short spin coherence times ($T_2^* < 100$ ns) at room temperature[62,63]. In epitaxial semiconductor QDs, spins (typically an electron or hole spin confined in the dot) experience a dense nuclear spin environment that tends to limit coherence. Hyperfine interactions with nuclear spins cause rapid dephasing of an electron spin's precession, giving a free induction of only a few nanoseconds[64]. Continued efforts in nuclear spin bath control through techniques such as nuclear spin polarization or feedback, together with material engineering strategies such as isotopic purification of semiconductors, aim to extend QD spin coherence close to the millisecond range[65,66].

Suppression of dephasing

Recent advances have substantially improved the suppression of phonon-induced dephasing in QEs (Box 1). One notable approach involves coherent two-colour excitation of InAs/GaAs QDs, which effectively decouples the exciton from its phonon bath[67]. Another promising strategy involves embedding QEs within phononic bandgap structures. By engineering the host semiconductor into a phononic crystal, a bandgap in the phonon density of states at targeted frequencies can be achieved. If the primary phonon coupling of the QE — typically in the gigahertz range for acoustic phonons — aligns with this bandgap, spontaneous emission of these phonons can be greatly suppressed[68,69]. Additionally, nanomechanical strain engineering strategies, such as creating a spatially varying strain gradient, could localize phonons away from emitter regions, acting as a phonon 'focusing lens'[70]. Another established approach consists in coupling QEs to high-finesse optical cavities, preferentially enhancing ZPL emission (discussed below).

In addition to optical techniques, dynamical decoupling and strain engineering have considerably enhanced spin coherence times. For instance, recent experiments using dynamical decoupling pulse sequences such as Carr–Purcell–Meiboom–Gill (CPMG) or XY8, applied to ensembles of negatively charged boron vacancies in hBN, have demonstrated an 100-fold increase in spin coherence time[63,71]. Si–V centres in diamond represent another example. By applying strain, the orbital degeneracy in Si–V centres can be lifted, substantially suppressing phonon-induced decoherence without requiring ultralow temperatures[72]. Another alternative is to identify colour centres with stronger spin–orbit coupling that remain robust at elevated temperatures, such as the tin–vacancy centre in diamond, which has recently been shown to host a high-quality spin–photon interface[73].

Inhomogeneity and spectral tuning

Inhomogeneous broadening (Box 1) is a major obstacle that arises from fabrication-induced disorder, strain fields, and fluctuations in the local electrostatic environment. This inhomogeneous broadening limits photon indistinguishability in emitter ensembles and complicates the creation of entanglement across multiple emitters. Therefore, the spectral tunability of QEs is crucial to enabling many-body entanglement. A widely used approach is electrostatic Stark tuning, implemented with microfabricated diode or gate electrodes that shift an emitter's transition through the quantum-confined Stark effect. This technique is well established for epitaxial QDs and routinely delivers tuning on the scale of millielectronvolts. For instance, single InGaAs/GaAs QDs show giant Stark shifts of several millielectronvolts under applied fields[74,75]. Lateral and vertical field configurations have been used to fine-tune excitonic transitions and even the exciton fine structure[75–77]. Analogous Stark control has been demonstrated for DBT molecules embedded in anthracene through permanent laser-induced tuning[78], with electrode integration enabling precise bidirectional control of molecular frequencies[79].

Many-body interactions, collective photon emission and quantum phase transition

Achieving entanglement among solid-state QEs requires engineering inter-emitter couplings that can withstand inhomogeneous broadening and environmental dephasing. Solid-state platforms offer a key advantage over cold atoms in this respect; the much higher emitter density can enhance interaction strengths by orders of magnitude, enabling a full hierarchy of collective phenomena, from entangled two-emitter states to mesoscopic ensembles exhibiting superradiant bursts and quantum phase transitions. These phenomena arise from the underlying mechanisms governing emitter–emitter interactions (Box 2).

Collective emission and entanglement in small emitter arrays

When the number of emitters is small and each emitter can be individually controlled, one can directly characterize the emergence of entangled states through their collective photon emission. In the simplest case of $N = 2$ emitters, dispersive coupling induces a coherent flip-flop interaction between the emitters, under which the single-excitation manifold splits into two entangled eigenstates: a symmetric 'bright' or 'superradiant' state and an antisymmetric 'dark' or 'subradiant' state[80]. The bright state carries an enhanced dipole moment and radiative rate, whereas destructive interference in the emission pathways of the dark state results in a suppressed decay rate (Box 2).

Spectroscopically, signatures of the entangled states therefore appear as a splitting of the optical resonance peak: the bright state typically shows a broadened, more intense spectral line, whereas the dark state appears as a narrower, weaker peak, with a splitting between them of the order of $2J$ (refs. 5,81,82) (Fig. 2a). Multidimensional ultrafast spectroscopy has also been used to directly probe multiexciton collective states, and oscillations in the interaction signal were observed as a function of pulse area, providing clear evidence of coherent exchange dynamics among Si–Vs in diamond[83]. Alternatively, the modified decay rates of the collective single-excitation states can also be observed directly from time-resolved emission dynamics[82,84].

A key requirement for the observation of these collective effects is nearly resonant emitters whose coupling J exceeds any difference in transition frequency or linewidth. Bringing multiple solid-state QEs into resonance is experimentally challenging because of inhomogeneous broadening (Box 1) (discussed above), but recent advances

Box 2 | Emitter interactions

Interactions in free space

Quantum emitters (QEs) in solids interact through distinct mechanisms depending on their separation. At very short distances below 1nm, direct wavefunction overlap leads to exchange interactions and Coulomb repulsion (see the figure, panel **a**). At larger separations, emitters interact through their dipole moments via the electromagnetic field (see the figure, panels **b** and **c**). At separations less than the transition wavelength, near-field dipole–dipole interactions, which scale with $1/r^3$, dominate. The far-field radiative coupling between emitters is highly tunable through the electromagnetic environment (see the figure, panels **d** and **e**), from the extreme confinement of plasmonic structures to the high-Q enhancement of dielectric cavities.

Together, these photon-mediated processes are captured by an effective master equation, where H_{eff} is the effective hamiltonian, ρ is the density operator and $\sigma^{\pm}$ are Pauli operators[297]:

$$\frac{\mathrm{d}\rho}{\mathrm{d}t} = -\mathrm{i}[H_{\mathrm{eff}}, \rho] + \sum_{ij} \Gamma_{ij}\left(\sigma_i^- \rho \sigma_j^+ - \frac{1}{2}\{\sigma_i^+\sigma_j^-, \rho\}\right), H_{\mathrm{eff}} = \sum_{ij} J_{ij}\,\sigma_i^+\sigma_j^- \qquad (1)$$

Both the coherent J_{ij} and dissipative Γ_{ij} coupling strengths are determined by the electromagnetic Green's function $\mathbf{G}(\mathbf{r}_i,\mathbf{r}_j)$, which describes the field at position $\mathbf{r}_i$ due to a dipole source at $\mathbf{r}_j$ (see the figure, panel **f**). The coherent coupling is given by the real part $J_{ij} = \mathrm{Re}[\mathbf{G}(\mathbf{r}_i, \mathbf{r}_j)]$ and enables excitation exchange between emitters through virtual photon exchange (see the figure, panel **b**). The dissipative coupling is given by the imaginary part $\Gamma_{ij} = \mathrm{Im}[\mathbf{G}(\mathbf{r}_i, \mathbf{r}_j)]$ and describes correlated spontaneous emission through real photon exchange, giving rise to collective superradiant and subradiant states (see the figure, panel **c**).

Interactions in a cavity

Structuring the electromagnetic field environment allows for the spatial tailoring of the Green's function. Photonic cavities enhance the couplings by concentrating the electromagnetic field, which can also be understood as modifying the local density of optical states. For a single QE, this enhancement is quantified by the Purcell factor $F_{\mathrm{P}} = \Gamma_{\mathrm{cav}}/\Gamma_{\mathrm{free}}$, where Γ_{free} is the free-space emission rate and Γ_{cav} is the emission rate into the cavity mode. Multiple emitters can interact through a cavity mode, leading to all-to-all connectivity.

Many-body effects from QE interactions

Interactions between QEs can lead to a multitude of many-body effects, including quantum phase transitions, effective nonlinearities and correlated photon emission. On-site interactions in lattices of QEs can realize Bose–Hubbard models (see the figure, panel **g**), leading to strongly correlated phenomena including quantum phase transitions arising from the competition between kinetic and interaction energies[298,299]. Strong photon-mediated near-field dipole–dipole interactions can also lead to the Rydberg blockade effect (see the figure, panel **h**), whereby the simultaneous excitation of multiple QEs to Rydberg states is suppressed across longer

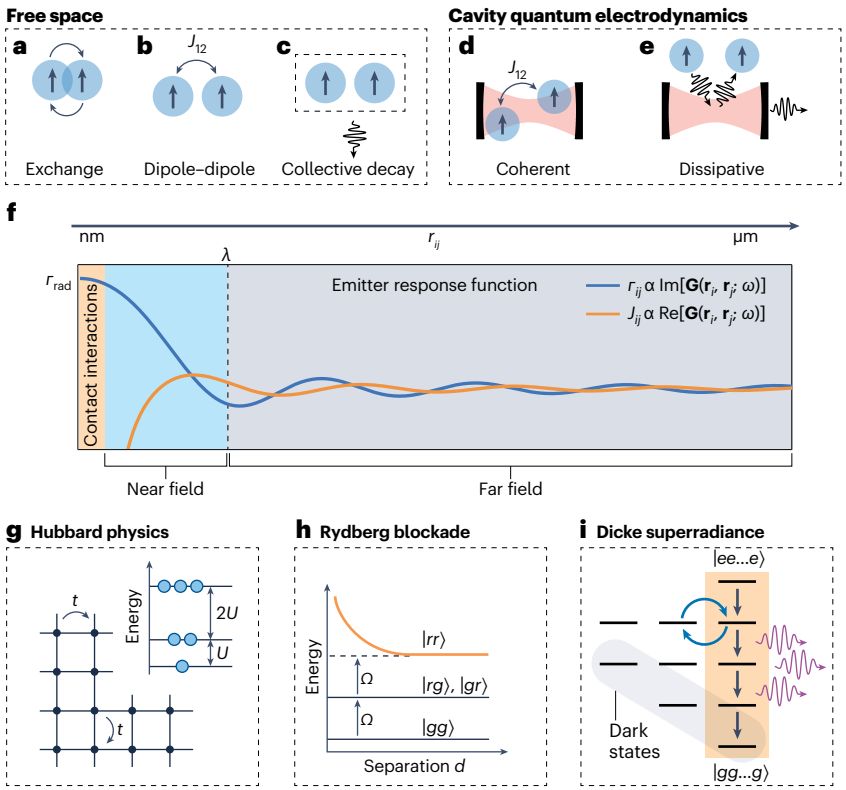

(continued from previous page)
distances[300]. Finally, dissipative interactions result in collective excitation structures of QE ensembles comprising both 'bright' states, displaying collectively enhanced coupling to the field, and 'dark' states, for which emission can be strongly suppressed or eliminated entirely[114] (see the figure, panel **i**).

have demonstrated its feasibility. One approach is to use electrostatic Stark tuning, for example by applying nanoscale electrodes to finely adjust the transition energies of pairs of organic emitters in a crystal[85]. Another approach is all-optical tuning, in which intense laser illumination can be used to induce local charge rearrangement and Stark shifts in organic nanocrystals to bring two embedded molecules into resonance[82] (Fig. 2a–d). In semiconductor systems, highly coherent epitaxial QDs can be tuned into resonance using magnetic fields[84].

An exciting frontier is controlling larger clusters of individually addressable emitters ($N > 2$) to explore richer many-body quantum dynamics. For $N = 3$, the permutationally symmetric subspace of collective states (Dicke manifold) already includes states with multiple excitations delocalized over the ensemble. By dynamically tuning one emitter in and out of resonance with others, one could drive transitions between Dicke states on demand. This capability could enable the realization of proposed tunable multiphoton emission schemes that rely on controlled coupling between collective bright and dark states[86–89]. Although a fully entangled state of $N = 3$ solid-state QEs has yet to be observed, a clear pathway requires the combination of precision tuning (to achieve spectral indistinguishability) and strong common coupling (through near-field or cavity mediation) (Box 2), followed by the use of coherent pulse sequences to navigate the multi-excitation state space. Another promising avenue of research is to build complexity by adding tunable disorder to the system, while retaining single-emitter control. For instance, few-emitter ensembles have been shown to display intriguing collective emission properties stemming from their coupling to multiple modes and the interplay between spectral and positional disorder[90,91].

Entanglement verification and coherent control

Harnessing the entanglement of a quantum many-body state requires accurate characterization methods. Quantum-state tomography is an experimental procedure to determine the amplitudes of a quantum state, from which a desired entanglement measure can be evaluated[92,93]. Although this method provides complete information about the state, the number of samples required for state tomography grows exponentially with the number of emitters, making it unsuitable for the many-body regime. Randomized measurement techniques[94] allow the study of mixed-state entanglement with far fewer samples[95,96]. In fact, they can provide a classical shadow[97] of the state: an approximate classical representation of the state from which properties such as entanglement entropies, expectation values of local observables and quantum fidelities can be obtained efficiently.

Under Markovian noise models, one can learn the quantum channel representing the noisy preparation using quantum process tomography[98,99]. This complete description of the channel again requires a number of samples that scales exponentially with the number of emitters. A common technique for state preparation is to start with an easy-to-prepare unentangled state and evolve it under a Hamiltonian or Lindbladian that can be written as a sum of local interaction terms. Recently, it has been shown that the Hamiltonian[100] or Lindbladian[101] coefficients can be inferred with a number of samples scaling only logarithmically with the number of emitters. Such scaling makes it possible to verify efficiently whether each local interaction term is being implemented to the desired precision.

Although these methods provide very fine-grained information, they require sample sizes or levels of experimental control that lie beyond the present capabilities of many platforms. Instead, several diagnostics of quantum behaviour have been developed that are currently broadly feasible to implement. Various experimental techniques can be used to confirm that few-emitter systems are indeed forming non-classical correlations and characterize their coherence. The most common approach is to use photon correlation measurements, as emitted photons statistics, characterized by the second-order correlation function $g^{(2)}(\tau)$, change markedly under collective emission. Specifically, an anti-dip at zero delay time that violates the upper bound $g^{(2)}(0) \leq (N-1)/N$ for emission from independent emitters provides a direct confirmation of inter-emitter correlations[102,103]. This feature has already been observed in several systems with $N = 2,3$ solid-state QEs[9,90,104–107]. However, recent theoretical work has shown that the observation of an anti-dip alone does not always constitute a reliable signature of superradiant behaviour, as qualitatively similar features can also be observed from ensembles of non-interacting QEs under realistic experimental conditions[108]. Nonetheless, two-photon correlation measurements still signal non-classical light and can even quantify how much improvement quantum-enhanced interferometry would offer compared with interferometry using a classical light source, as they allow the efficient computing of the quantum Fisher information of the emitted photons[89].

Hong–Ou–Mandel interference is the benchmark for verifying mutual coherence between distinct emitters. It has been used to verify coherence between remote and independent QDs: for example, two separate QDs can be tuned into resonance using strain[109] or electrical Stark tuning[110]. Applying sequences of ultrafast pulses enables probing of the phase coherence and manipulation of the joint state of the coupled emitters. Ramsey interference experiments, in which two $\pi/2$ pulses separated by a variable delay are applied, can reveal coherent oscillations between the collective eigenstates (superradiant versus subradiant) as an oscillatory modulation in emission or absorption[111,112]. Such experiments are analogous to optical Ramsey control and confirm that the two-emitter system retains quantum phase coherence.

Collective phenomena in large ensembles

Even when dealing with large numbers of solid-state emitters that are not individually addressable, striking many-body effects can emerge from their mutual interactions. In the many-body regime, highly excited ensembles of interacting QEs are predicted to display Dicke superradiance[113,114], whereby an ensemble of N QEs emits a short burst of radiation with a peak intensity $\propto N^2$. Extending this proposal, numerous theoretical works have demonstrated that long-range photon-mediated

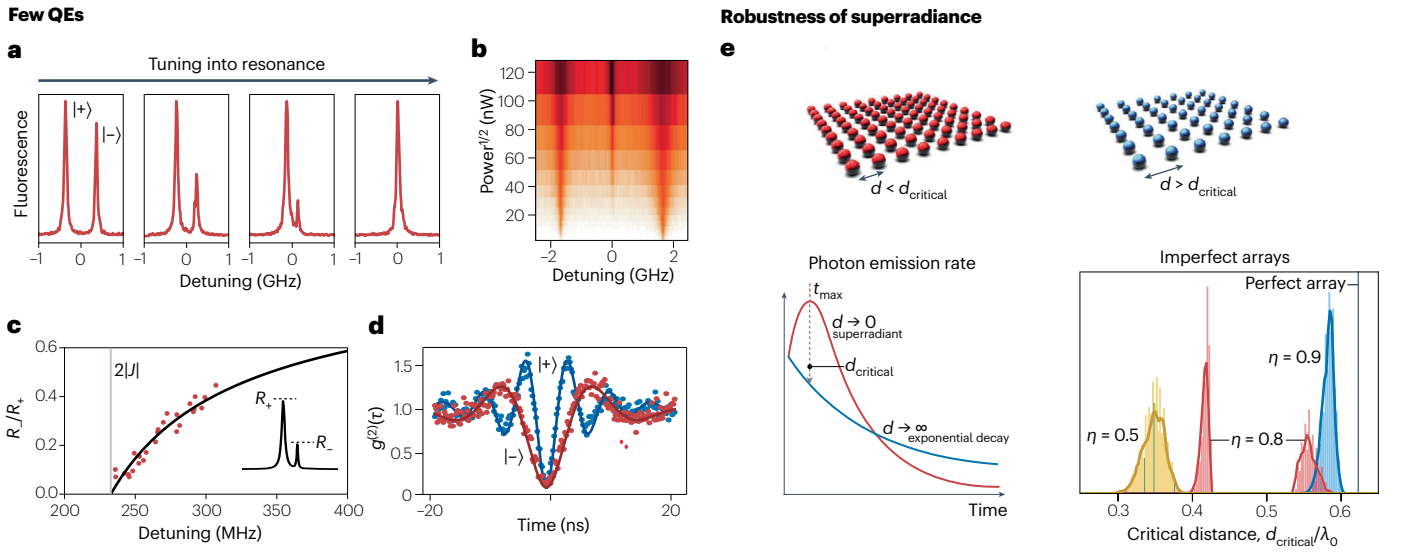

interactions can be used to engineer many-body superradiance in extended systems, such as subwavelength free-space QE arrays[115–117] (Fig. 2e) or QE ensembles coupled to low-dimensional fields[118]. Notably, the hallmark feature of the superradiant burst is robust in such settings, even in the presence of multiple competing collective decay channels and positional disorder (Fig. 2e), and it can be predicted solely from the coherence properties of the system in the initial stages of the collective decay[119,120]. Dense solid-state QE arrays, including molecules, colloidal QDs and 2D TMDs, are ideal platforms to experimentally test these predictions. For example, 3D superlattices of nanocrystals have been shown to support superradiance emission and form many-body excitonic states[121–125] (Fig. 2f,g).

The key challenge in the many-body regime is the characterization of the emergent entanglement structure and the understanding of how

Fig. 2 | Many-body entanglement and collective emission in solid-state quantum emitter systems. a, Spectra of the superradiant $|+\rangle$ and subradiant $|-\rangle$ single-excitation states of two subwavelength-spaced organic molecules, showing an extinguishing of the subradiant linewidth as the molecules are tuned into resonance. **b**, Associated fluorescence spectrum, displaying an additional two-photon peak at sufficiently large excitation power associated with the fully excited two-emitter state. **c**, Ratio of the heights of the subradiant (R_-) and superradiant (R_+) peaks for varied detuning. **d**, Photon correlation functions for the states $|\pm\rangle$, displaying modified Rabi frequencies and lifetimes. **e**, Theoretical prediction of many-body superradiance in 2D subwavelength quantum emitter (QE) arrays with interatomic spacings above (blue) and below (red) the critical threshold for superradiance. The emergence of a superradiant burst as $d \to 0$ is found to be robust against positional disorder and experimental imperfections, such as below-unity filling fraction (η) of the array. **f**, Electron micrograph of a 3D perovskite quantum-dot superlattice. **g**, Photon correlation function $g^{(2)}(\tau)$, showing photon bunching at zero delay as a signature of superradiance in the system shown in panel **f**. **h**, Moiré excitons in a WSe_2/WS_2 bilayer mapped to an extended Bose–Hubbard model with strong on-site exciton–exciton interaction U_{ex} and long-range dipolar coupling V_{DD}. **i**,**j**, Schematic potential (panel **i**) and time-resolved transport of the system at various injected exciton densities ($\langle N_0\rangle = 3$ (blue), $\langle N_0\rangle = 1$ (pink) and $\langle N_0\rangle = 0.4$ (yellow)) (panel **j**) reveal a crossover to a correlated (Mott-insulating) phase at high filling $\upsilon_{ex} \gtrsim 1$, evidenced by a suppressed mean-squared displacement (MSD) and a turning point in the dynamics, as described by a piecewise linear (PWL) fit. Panels **a**–**d** adapted from ref. 82, Springer Nature Limited. Panel **e** reprinted from ref. 115, CC BY 4.0. Panels **f** and **g** adapted from ref. 121, Springer Nature Limited. Panels **h**–**j** adapted from ref. 143, Springer Nature Limited.

it can be harnessed as a resource. For example, distinguishing genuine many-body correlations from pairwise correlations remains an experimental hurdle. On the theoretical side, extensive work has been dedicated to characterizing the correlation structure that emerges in the photonic state emitted by a superradiantly decaying QE ensemble[86,87]. Superradiance generates photonic many-body states that achieve Heisenberg scaling of the quantum Fisher information[89,126], thereby constituting a valuable potential resource for quantum-enhanced interferometry. Suitably tailored collective light–matter coupling allows, in principle, for the realization of large decoherence-free subspaces, spanned by collective states decoupled from the field[127,128], providing a promising setting for the storage[129–131] and processing[132–135] of quantum information. However, although such subspaces are naturally protected against collective dissipation, dark states may still be subject to other decoherence mechanisms, such as local radiative or non-radiative decay.

Quantum phase transitions

With strong interactions, a dense ensemble of QEs can enable investigations of quantum phase transitions and quantum simulation[136,137]. A particularly exciting platform for exploring strongly correlated many-body states of light and matter is moiré excitons in van der Waals heterostructures because of their strong exciton–exciton interactions[138,139]. For example, when two semiconducting monolayers (such as WSe_2 and WS_2) are stacked with a slight twist or lattice mismatch, they form a long-period moiré pattern that creates an array of localized moiré excitons. The moiré potential and the exciton interaction can be tuned by modifying the twist angle and materials combination to realize different regimes of Bose–Hubbard physics (Box 2). Individual moiré exciton traps have already shown single-photon emission, confirming that they behave as quantized emitters[140]. Bose–Hubbard model physics has also been realized using moiré excitons, and recent experiments have begun to reveal new many-body phases driven by their mutual interactions[141–143]. Long-range dipolar repulsion freezes the motion of the Mott insulator phase for more than 70 ns (Fig. 2h–j). This frozen-dynamics behaviour, arising from strong repulsive interactions, is characteristic of highly coherent systems and was previously realized exclusively in ultracold gases[143]. Compared with cold-atom quantum simulation platforms[144], solid-state QEs can realize stronger, longer-range interactions. For future studies, a priority is to control many-body interactions (Box 2) to realize diverse quantum phases. At the same time, it will be crucial to quantify and mitigate dephasing, such as phonon coupling, to determine how these dynamics affect phase diagrams and collective behaviours.

Photon-mediated many-body interactions

A core requirement for entangled states of light and matter is efficient coupling between QEs and well-defined photon modes. Nanophotonic integration offers the capability to engineer light–matter interactions to achieve scalable distributed entanglement[24,27,145,146]. Magnified coupling to a specific mode can be achieved either by increasing spontaneous emission into the desired mode or by suppressing spontaneous decay into free-space modes. If the total decay rate is increased, radiative decoherence can be accelerated to exceed dephasing from other sources, increasing the optical coherence of the emitter[147]. When emitters are coupled to a guided mode, the total collection efficiency of photons from the emitter can be enhanced[148–150]. This enhancement is crucially important for generating entangled light, which is sensitive to photon loss. In the strong-coupling limit, a QE becomes a strong nonlinear element even at the single-photon level[151–153].

In the multiemitter regime, coherent exchange of excitations through a shared cavity mode mediates effective emitter–emitter coupling, extending the interaction length scale from near-field nanometres to micrometres (and even beyond along guided modes) (Box 2). By optically exciting the superradiant mode of multiple QEs and projecting onto their two-spin ground states, one can prepare an entangled spin–spin state. This approach is analogous to cavity-mediated gates demonstrated in atomic systems and is a promising route towards deterministic multiqubit logic in solid-state devices. Driving the two-photon transition of two non-identical QEs can dissipatively stabilize the system into nearly maximally entangled stationary states[154]. As nanofabrication and control continue to improve, direct entangling gates between solid-state qubits in a photonic cavity or waveguide will become feasible.

Nanophotonic resonators and waveguides

In the fast cavity regime, the enhancement of the light–matter interaction is quantified by the Purcell factor $F_P = \frac{3}{4\pi^2}\left(\frac{\lambda}{n}\right)^3 \frac{Q}{V}$, where λ is the resonance wavelength, n is the refractive index, Q is the cavity quality factor and V is the mode volume. The quality factor is proportional to the photon lifetime in the cavity. The mode volume is a measure of the confinement of a photon in the cavity, with a smaller V resulting in a higher emitter–photon interaction strength. Ring resonators and disk resonators rely on highly symmetric circular geometries to achieve exceptionally high quality factors reaching the hundreds of millions in silicon nitride platforms[155–158]. The trade-off for these high Q values is a higher mode volume, which is generally tens of cubic wavelengths or larger. Photonic crystal cavities use photonic bandgaps combined with total internal reflection to confine light, allowing both high Q factors

from low-loss dielectric mirrors and very small mode volumes. One-dimensional photonic crystal cavities confine light using a periodic structure along one axis (a nanobeam or nanopillar) combined with total internal reflection in the other two directions. Two-dimensional photonic crystal cavities use a 2D lattice of holes in a membrane slab to provide in-plane confinement through a photonic bandgap, whereas vertical confinement comes from total internal reflection. Defects in the periodicity can localize the photonic mode and concentrate the electromagnetic field within a small mode volume. Photonic crystal cavities with $Q > 100{,}000$ and mode volumes of the order of a cubic wavelength have been demonstrated[159]. Importantly, photonic crystal cavities such as nanobeam cavities can be strongly coupled to guided modes for efficient outcoupling of light while maintaining high Q factors.

Light–matter interactions can be enhanced by slowing the group velocity using photonic crystal waveguides, with demonstrated slow-down factors up to 300 (ref. 160). For a photonic crystal waveguide constructed with a line defect in a 2D photonic crystal, emitters experience strong suppression of free-space emission, leading to high collection efficiency even with modest increases of emission rate. Photonic crystal waveguides also offer broadband operation, providing versatility across different wavelength ranges. Furthermore, they can be engineered to support chiral light–matter interactions in which light propagation becomes unidirectional owing to optical spin–orbit coupling[161,162]. Such chiral coupling enables applications in non-reciprocal photonic devices (such as in optical isolators and circulators) and establishes directional coupling between multiple emitters embedded in the same waveguide, forming cascaded quantum systems.

Plasmonic structures exploit collective oscillations of surface electrons in metallic nanostructures to confine electromagnetic energy below the diffraction limit and produce strong, localized field enhancements[163]. Purcell factors upward of 10,000 are achievable in structures such as nanoparticle-on-mirror cavities or nanoparticle antennas[164–166]. A major limitation of localized plasmonic systems is that much of the Purcell enhancement is non-radiative: energy stored in plasmonic modes is often converted into heat through ohmic losses instead of being emitted as photons. One strategy to mitigate this effect is to use hybrid dielectric–plasmonic cavities, which combine the high Purcell factors of plasmonic resonances with low-loss dielectric structures, enabling efficient photon outcoupling before energy is dissipated as heat[167]. Another approach involves plasmonic nanoparticle lattices, where localized surface plasmon resonances are coupled to the diffractive orders. In addition, careful material choices, such as using low-loss metals[168,169], can further mitigate material instability and thermal dissipation.

Modified dielectric cavities can also achieve extreme confinement, reaching mode volumes as low as $7 \times 10^{-5}(\lambda/n)^3$ (ref. 170). Another emerging approach generates photonic structures through global topological optimization, in contrast to adiabatic modifications of photonic crystals used to create defect states. Topology-optimized (or inversely designed) cavities have demonstrated similar mode volumes of $3 \times 10^{-4}(\lambda/n)^3$ with small device footprints[171].

Across all platforms, materials and integration are of critical importance. High-index-contrast materials tighten confinement but may increase loss; embedding the emitter during growth maximizes light–matter coupling but restricts the choice and density of QEs, whereas hybrid integration eases assembly at the expense of positioning accuracy and coupling strength. The optimal choice depends on target applications, uniform coupling across many emitters, bandwidth versus coherence, and the required degree of programmability for many-body interactions.

Cavity quantum electrodynamics with multiple emitters

Cavity quantum electrodynamics (QED) with multiple QEs coupled to a common photonic mode unlocks collective phenomena central to many-body quantum optics. A remarkable feature of cavity and waveguide QED is that QEs can interact coherently without requiring nanometre-scale separations (Box 2). The resulting photon-mediated interactions, described by the Tavis–Cummings model, give rise to collective eigenstates and modified decay rates. These effects were initially observed in atomic ensembles and have now been realized in solid-state platforms as well[129,172–177].

The behaviour of two emitters in a cavity can be classified into three regimes (Fig. 3a): first, when the emitters are detuned from each other but near resonant with the cavity, they act independently and each experiences ordinary Purcell enhancement; second, when the emitters are resonant with each other and the cavity, they form symmetric (superradiant) and antisymmetric (subradiant) collective states, with the superradiant state decaying at an enhanced Purcell rate while the subradiant state decouples from the cavity mode; and third, when the emitters are resonant with each other but detuned from the cavity, they couple dispersively through a virtual photon exchange, leading to a dipole–dipole interaction that shifts the symmetric and antisymmetric states by the exchange rate $\pm J_{12}$, producing a splitting of $2J_{12}$.

Solid-state demonstrations of radiative emitter–emitter coupling in cavity QED were initially achieved using Si–V centres in diamond. For example, two Si–V centres embedded in a nanophotonic diamond cavity were each strongly coupled to the high-Q cavity mode[5] (Fig. 3b). The common cavity mode induced a coherent interaction between the emitters, manifesting as a pronounced splitting in the optical spectrum owing to coherent dipole–dipole coupling mediated by cavity photons. By using the electronic spin of each Si–V as a controllable qubit, the interaction could be turned on and off by tuning one emitter in and out of resonance. V_{Si} centres have also been integrated into thin-film silicon carbide microdisk resonators fabricated on SiC-on-insulator platforms[90]. The high-Q whispering-gallery modes of these microdisks provided strong Purcell enhancement, yielding single-emitter cooperativities up to 0.8. When two V_{si} centres were coupled to the same resonator mode, their joint emission exhibited superradiant bunching in photon correlation measurements, confirming collective radiative decay (Fig. 3c).

Cavity QED with two epitaxial QDs has also been demonstrated. A foundational step towards multiemitter applications was the observation of coherent coupling and collective superradiant and subradiant emission from deterministically positioned QDs in a nanophotonic waveguide[84] (Fig. 3d). These experiments showed clear signatures of photon-mediated interactions, including enhanced collective emission rates (superradiance). By tuning individual QD emission wavelengths through electrostatic gating, magnetic field or strain engineering, it becomes possible to map out interaction-driven transitions between collective eigenstates. Steady-state subradiant emission from two InAs QDs embedded in a low-Q, highly directional circular grating Bragg cavity has also been achieved, where the subradiant-state population dominated the steady state with a highly negative cooperativity[178]. Long-range energy transfer between two InAs QDs embedded in a photonic crystal waveguide has further been demonstrated by tuning the emitters into resonance and measuring intensity autocorrelation, yielding $g^{(2)}(0) = 0.94$ (ref. 179).

In addition to colour centres and QDs, recent work has demonstrated the compatibility of organic molecules with nanophotonic resonators.

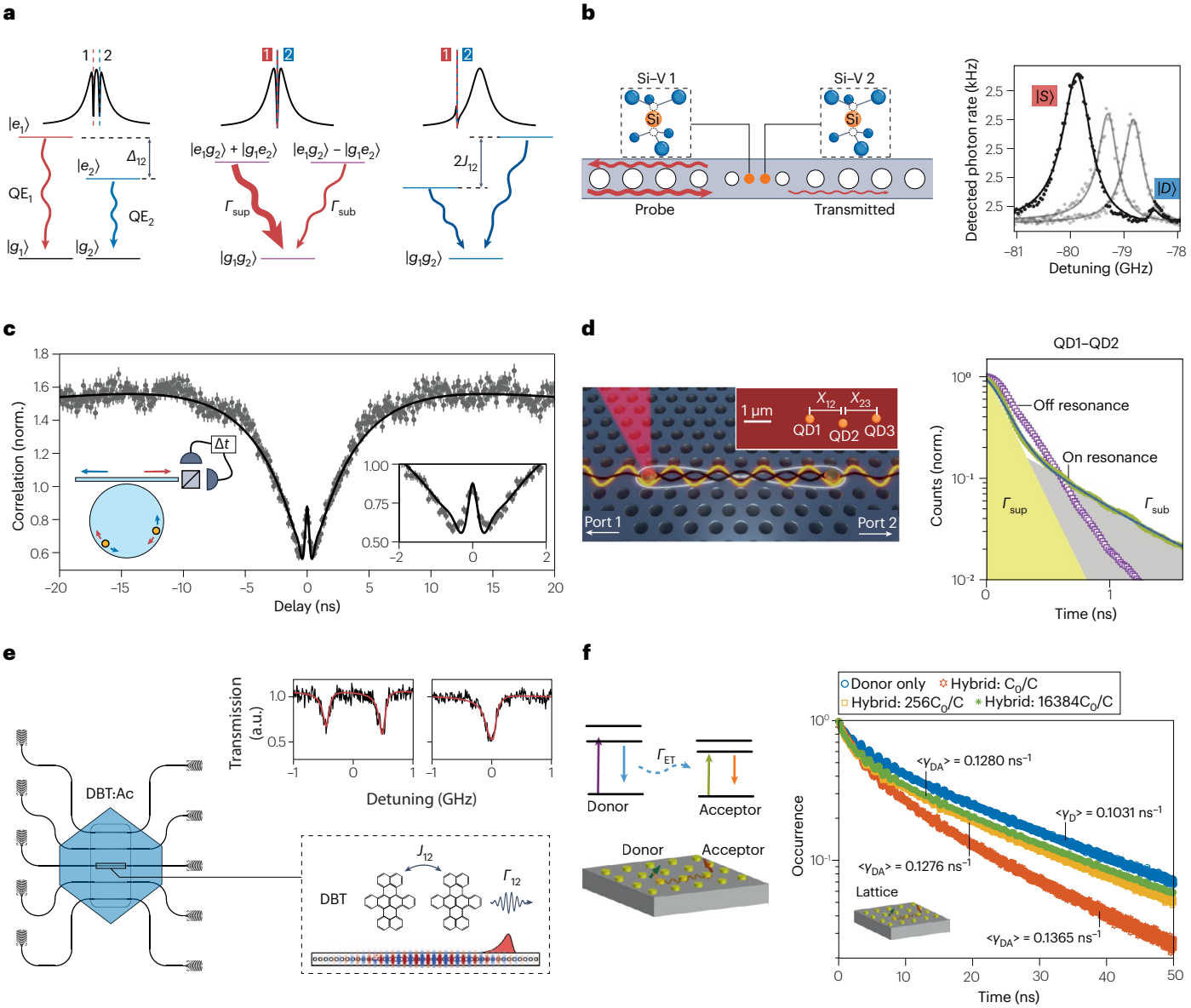

Fig. 3 | Collective interactions of multiple solid-state quantum emitters in nanophotonic environments observed across molecular, quantum-dot and colour-centre platforms. a, Schematic cavity transmission spectra and energy-level diagrams illustrating three regimes: two emitters off resonance with each other but near-resonant with the cavity, decaying independently (left); emitters resonant with each other and with the cavity (dissipative regime), where superradiant and subradiant collective states form (middle); and emitters resonant with each other but detuned from the cavity (dispersive regime), where coherent dipole–dipole interactions split the symmetric and antisymmetric states (right). **b**, Cavity-mediated interaction of two silicon–vacancy (Si–V) centres in a diamond nanocavity with emitter–cavity detuning, showing formation of bright $|+\rangle$ (superradiant, $|+\rangle$) and dark (subradiant $|-\rangle$) collective states. **c**, Superradiant emission observed from two V_{Si} centres in a thin-film SiC microdisk cavity manifested through bunching in photon correlation measurements. **d**, Observation of superradiant and subradiant emission from pairs of quantum dots (QDs) deterministically positioned in a nanophotonic waveguide (separated by X_{12} and X_{23}, respectively), mediated by long-range radiative coupling. Superradiant and subradiant dynamics are reflected in the decay rates Γ_{sup} and Γ_{sub}, respectively. **e**, Two dibenzoterrylene (DBT) molecules coupled to a 1D photonic crystal cavity, interacting either dissipatively through the cavity mode (Γ_{12}) or dispersively through dipole–dipole coupling (J_{12}). **f**, Long-range dipole–dipole interactions mediated by a plasmonic nanoparticle lattice, manifested through decay lifetime γ of donor molecules in the presence (γ_{DA}) and absence (γ_D) of acceptors. Acceptor concentration was tuned through the dilution factor C/C_0. QE, quantum emitter. Panel **b** reprinted with permission from ref. 5, AAAS. Panel **c** reprinted from ref. 90, CC BY 4.0. Panel **d** reprinted with permission from ref. 84, AAAS. Panel **f** reprinted with permission from ref. 189, ACS.

For example, lifetime-limited DBT molecules embedded in polyethylene films have been tuned into resonance while coupled to disc resonators, by using electrodes to control their transition energies[180]. DBT molecules in anthracene crystals have also been coupled to nanobeam

cavities, where permanent optically induced Stark shifts gave rise to resonant coupling in both dissipative and dispersive regimes[181] (Fig. 3e). The high density achievable with molecular emitters can, in principle, enable coherent coupling among large ensembles of emitters (>3).

Finally, plasmonic cavities have also been used to mediate many-body entanglement. An isolated nanoparticle antenna can tightly confine the light field and support pairwise or small-scale entanglement among a few emitters, although the efficiency depends heavily on emitter number and position owing to rapid near-field decay[182–184]. The uniformity of the field distribution can be improved by using nanoparticle-on-mirror cavities with nanoscale dielectric gaps that produce spatially homogeneous fields[185,186]. Such designs enable multiple QEs to experience comparable coupling conditions and consequently enhanced overall coherence[187,188]. Plasmonic nanoparticle lattices support delocalized surface lattice resonances to facilitate coherent interactions across many unit cells and over hundreds of nanometres. For instance, silver nanoparticle arrays coupled to donor and acceptor dye molecules exhibited resonance energy transfer that persisted up to about 800 nm of mean donor–acceptor separation — nearly two orders of magnitude larger than free space[189] (Fig. 3f). Such long-range dipole–dipole coupling mediated by surface lattice resonances open up opportunities for exploring collective phenomena such as superradiance and correlated photon emissions[190]. Moreover, when the lattices are strongly coupled with emitters, the formed exciton-polaritons inherit the nonlinearity of excitons and can achieve polariton lasing and condensation at room temperature[191–194].

Collectively, these results demonstrate that, with nanophotonic integration, even solid-state emitters separated by many wavelengths can interact strongly[195,196] (Fig. 3). In future studies, pushing cavity QED from pairs to larger ensembles of solid-state QEs hinges on making the collective Hamiltonian programmable and homogeneous while keeping each emitter transform-limited. Reaching that level of control will require further developments in deterministic emitter placement, active frequency tuning and nanophotonic strategies that enhance light–matter coupling and collection efficiencies.

Photon nonlinearity

In addition to serving as mediators of entanglement between emitters, photons can also carry quantum entanglement as resource states themselves. Therefore, strong photon–photon interactions at the single-photon or few-photon level represent a milestone in quantum optics. Achieving strong photon–photon interactions enables all-optical analogues of transistors and logic gates at the quantum level, as well as deterministic entangling operations between photons[197,198]. Photons do not naturally interact with each other in free space or linear media, so achieving photon nonlinearities requires mediating interactions through matter. Early theoretical proposals showed that embedding resonant emitters or nonlinear media in optical systems could induce an effective photon–photon interaction[197,199]. The main underlying mechanism is an excitation blockade that can originate either from the saturation of a single or a few two-level emitters, or from strong and long-ranged interactions, as can be mediated by Rydberg states (Rydberg blockade) (Box 2). In the strong light–matter coupling limit, the nonlinearity of the emitters can be translated into a photon–photon interaction that can even give rise to a photon blockade, in which one photon in a nonlinear medium prevents a second photon from entering[198,200]. These ideas have laid the groundwork for quantum nonlinear optics, suggesting that a single photon could switch or modulate another.

Large photon nonlinearities require both a strong light–matter interaction that maps each photon onto a matter excitation and a strong matter–matter interaction so that one excitation can considerably shift or block a second. By simultaneously engineering high-cooperativity photon coupling (using microcavities, waveguides or plasmonic confinement as discussed in the previous section) and enhancing emitter–emitter interactions (through Rydberg excitation, moiré trapping or dipole–dipole coupling) (Box 2), recent experiments have pushed nonlinear responses into regimes previously accessible only with intense light fields[201].

Polaritons with Rydberg excitons

One of the most advanced platforms for single-photon-level nonlinearity is based on ultracold atomic ensembles with Rydberg excitations[197,202]. In this approach, photons are coupled using electromagnetically induced transparency to highly excited Rydberg states of atoms, forming Rydberg polaritons. When one photon excites a Rydberg atom, it can block the excitation of nearby Rydberg atoms within a 'blockade radius', effectively causing two photons within that range to interact strongly. This mapping of Rydberg-atom interactions onto photons has enabled a host of quantum nonlinear optical effects. Notably, it allows single photons to phase-shift or attenuate other photons[203,204] and even implement two-photon gates[205,206]. The trade-off, however, is that such experiments typically require ultracold temperatures or vacuum systems and precise control of atomic states[207–209].

In the solid-state realm, an exciting development is the use of Rydberg exciton-polaritons in semiconducting materials to achieve photon nonlinearity (Fig. 4a,b). Exciton-polaritons arise in semiconductors or 2D materials when an exciton strongly couples to a cavity photon, forming a hybrid quasiparticle. Polaritons can interact with each other through their excitonic component, and if these interactions are strong enough, quantum nonlinear effects analogous to those in atomic systems can emerge. Figure 4b shows a small experimental dip in $g^{(2)}(\tau)$ at $\tau = 0$ ($g^{(2)}(0) < 1$), demonstrating the onset of a polaritonic excitation suppression in a semiconductor quantum-well microcavity[210]. Rydberg excitons in bulk semiconductors have been pursued as an analogue to atomic Rydberg gases, where the excitation suppression can potentially be greatly enhanced[211]. Cuprous oxide (Cu_2O) has emerged as one of the most successful material candidates: it supports Rydberg excitons with principal quantum numbers up to $n = 30$, whose diameters can approach 1 µm (Fig. 4c). These Rydberg excitons in Cu_2O have extremely large electric transition dipole moments, leading to exciton–exciton interaction strengths orders of magnitude larger than those of ground-state excitons. Giant Rydberg excitons in Cu_2O have been experimentally demonstrated in bulk crystals[212–214], synthetic thin films[215,216] and 2D arrays[217]. Their power and temperature-dependent characteristics, as well as their controllability through microwave fields[218] have been investigated[219–221], providing important insights into the linear and nonlinear optical properties of this system. Strong light coupling to Cu_2O Rydberg excitons up to $n = 6$ has been achieved, creating Rydberg exciton-polaritons (Fig. 4d). Kerr-type optical nonlinearities arising from the Rydberg blockade effect in a Cu_2O microcavity have also been demonstrated[222]. The polariton resonance frequency was found to shift depending on the polariton density (Fig. 4e), an effect attributed to the Rydberg exciton blockade.

Monolayered TMDs host tightly bound excitons with large binding energies, and they can sustain polaritons even at room temperature[223,224]. Although larger binding energies are typically

associated with smaller interaction strengths, the 2D material geometry offers unique opportunities for the realization of photon–photon interactions. Combining monolayer TMD excitons with a microcavity[225] or a two-colour excitation scheme[226] has been proposed as a way to exploit the material structure to produce light with quantum mechanical statistics. The formation of polaritons based on the 2*s* exciton in monolayer WSe_2 has been experimentally demonstrated, and their nonlinear properties have been compared with those of polaritons formed from the ground 1*s* exciton[227]. Because excited-state excitons are larger in size, their mutual interactions are stronger. However, the enhanced nonlinearity of the 2*s* state still falls short of the 'quantum blockade' regime. Rapid dephasing and strong phonon scattering in TMDs pose considerable challenges in accessing higher Rydberg states, representing a major obstacle to achieving single-photon nonlinearity.

Dipolar and moiré exciton-polaritons

Another promising strategy to strengthen exciton–exciton interactions is to use excitons with a permanent electric dipole moment, enabling dipolar interactions. One such example is interlayer excitons, which can form in van der Waals bilayers of TMDs owing to the separation of an electron–hole pair across the layer interface. Large nonlinear interactions between interlayer exciton-polaritons have been demonstrated with bilayer MoS_2 (ref. 228) (Fig. 4f–h). As described previously, moiré excitons feature reduced bandwidth and very large nonlinearity because of spatial localization, strong on-site interactions and long-range dipolar coupling. Moiré exciton-polaritons also exhibit enhanced and electrically tunable nonlinearities[229] (Fig. 4i,j). The moiré approach offers a promising route towards scalable quantum nonlinear optics on a chip with an array of interacting polariton sites that could mimic a strongly correlated photonic lattice, all in a 2D solid.

Strategies to further enhance interactions

Taking inspiration from ultracold atomic gases, researchers have sought Feshbach resonances in excitonic systems, where a two-particle scattering interaction is greatly enhanced by the presence of a bound state at nearly the same energy[230]. A bound state of two excitons is known as a biexciton, and a bound state of an exciton and an extra charge is known as a trion. In GaAs quantum wells, when two polaritons with opposite spin are tuned into resonance with the biexciton energy by adjusting the cavity detuning, their effective interaction switch from weakly repulsive to strongly attractive and then back to repulsive as the resonance is crossed[230]. In TMD monolayers, biexcitons with binding energies of the order of 20–40 meV exist as well, so in principle, a similar tuning could be achieved by bringing the polariton or two-exciton energy near the biexciton state. Owing to the larger binding energy, the resonance condition in TMDs might be achieved at higher temperatures or with smaller detunings. Moreover, recent theoretical proposals suggest using trion states in a controlled way to induce Feshbach-like tunability[231,232]. To enhance light–matter interaction, using photonic structure to further confine the photons or slow down photon propagation would be desirable. TMDs could offer a simpler route to implement such structures, as their atomically thin nature means they can be transferred onto virtually any photonic platform without perturbing the mode structure. This 2D flexibility has enabled TMD strong coupling in a wide variety of architectures, from planar cavities and waveguides to nanogaps and plasmonic antennas[233,234].

Generation and characterization of cluster and graph states

Graph states are special types of entangled quantum states that can be visualized as graphs, with the vertices representing the qubits and the edges between connected qubits representing entanglement links (reviewed previously[235]) (Fig. 2). In particular, the collection of nodes and edges mathematically describes a complete set of correlation observables that uniquely determine the corresponding graph state. The best-known graph state is the 'cluster state', a 2D square graph, which was shown to be a universal resource for quantum computing in the seminal paper by Raussendorf and Briegel[236]. Photonic graph and cluster states could overcome challenges associated with photonic quantum computing and quantum repeaters. Generating large photonic cluster or graph states has been difficult to scale. The conventional approach uses probabilistic linear-optical methods; independent single photons or entangled photon pairs, typically generated through nonlinear processes such as spontaneous parametric down-conversion or spontaneous four-wave mixing, are interfered, and a subset of them measured, to 'stitch' photons into a cluster state[237]. Standard objections to the probabilistic approach have been related to, first, the intrinsically low efficiency of these entangled photon pair sources, and second, the probabilistic nature of the approach (the protocol succeeds conditional on certain low-probability measurement outcomes); related to this, the fusion gates for photons are themselves probabilistic[237]. These challenges are in part addressed by pumping the sources with an ultrafast pump laser, which increases the entangled pair generation rate[238], as well as by reusing the contracted graph states following a failed fusion gate allowing the gate to be reattempted, which reduces the resource requirements (in terms of entangled photon pairs) for a successful fusion event. Although it has enabled pioneering demonstrations of photon cluster states[239], this approach remains difficult to scale[240,241] without combining it with deterministic methods, as done in recent experiments[242,243]. Recent research has therefore turned to a combination of probabilistic and deterministic protocols[244] or fully deterministic sources: solid-state QEs with spin–photon interfaces that can emit or mediate entanglement on demand[245–248]. In principle, such an approach could be done with single or multiple QEs.

Generation of cluster states at the spin–photon interface

Experiments with atomic emitters have improved the quality of the gates and have demonstrated a record number of photons in linear cluster states[249] and Greenberger–Horne–Zeilinger (GHZ) states. However, the naturally longer timescales and technically challenging operation of atomic systems limit their generation rate and scalability. Later experiments with QDs improved on these limitations[7] (Fig. 5a–f), including recent work with a cavity that enhances emission efficiency[8,250] (Fig. 5a–d). These results provide clear evidence that solid-state QEs can rapidly generate photonic graph states while offering the potential for device integration.

Aside from epitaxial QDs, colour centres are particularly well suited for generating graph states beyond a 1D cluster state owing to the presence of nearby nuclear spins with optically accessible initialization, control and readout, all mediated through the defect spin. In addition, the ability to perform conditional gates between the spin defect and nearby nuclear spins has been demonstrated both for strongly and weakly coupled nuclear spins. The nearby strongly coupled nuclei can be addressed directly by using the Overhauser shift of the defect energy levels, resulting in relatively fast entangling gate times. By contrast, entangling gates with weakly coupled nuclei[251,252] requires applying a

Nonlinearity

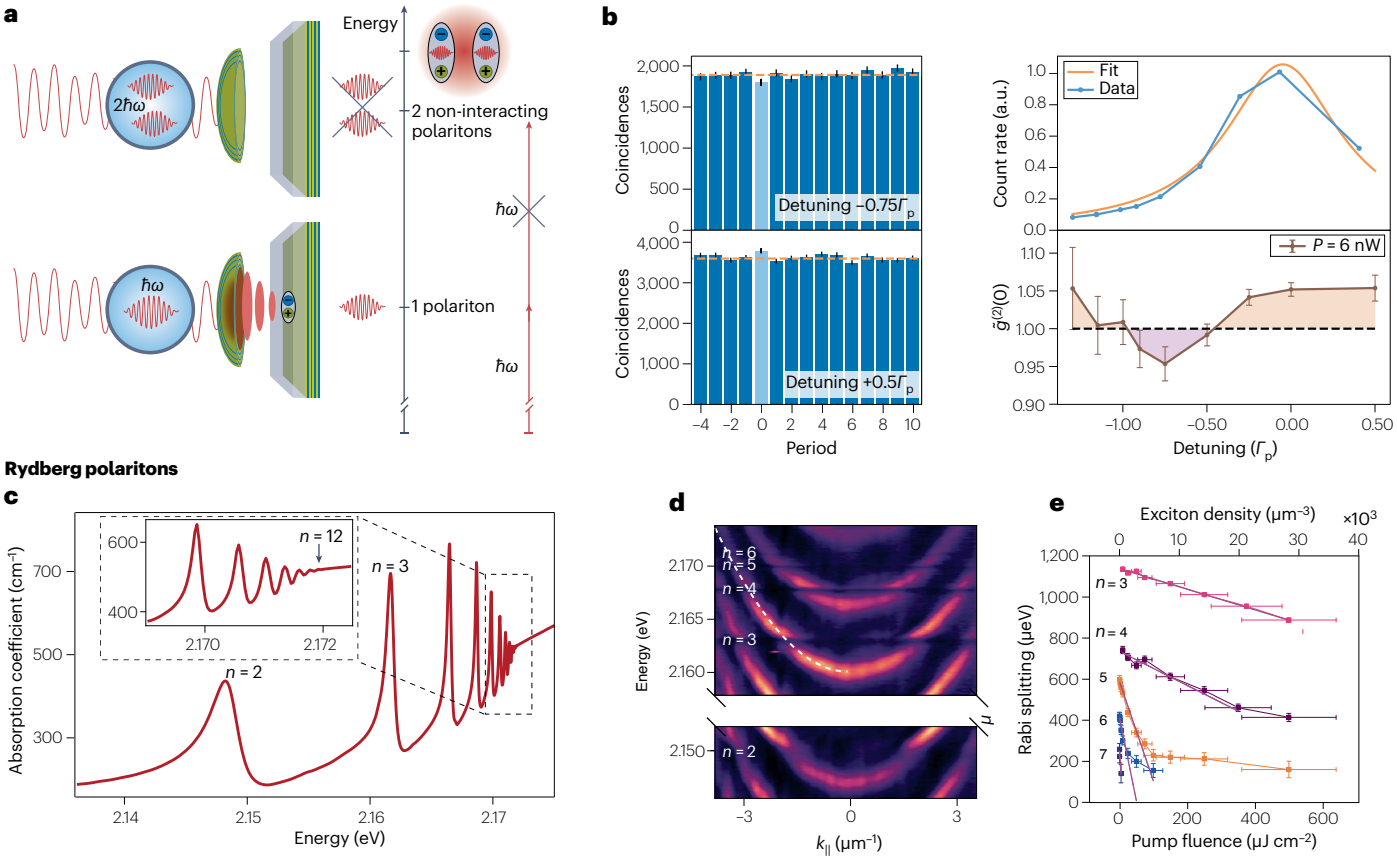

Rydberg polaritons

Dipolar polaritons

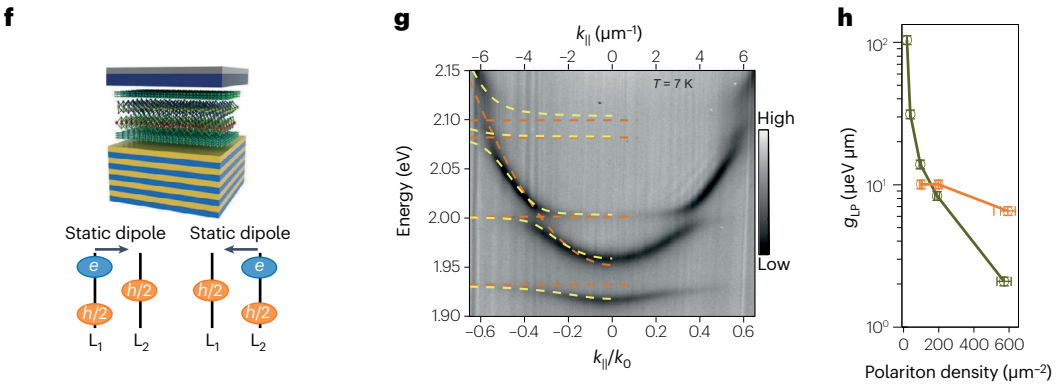

Moiré polaritons

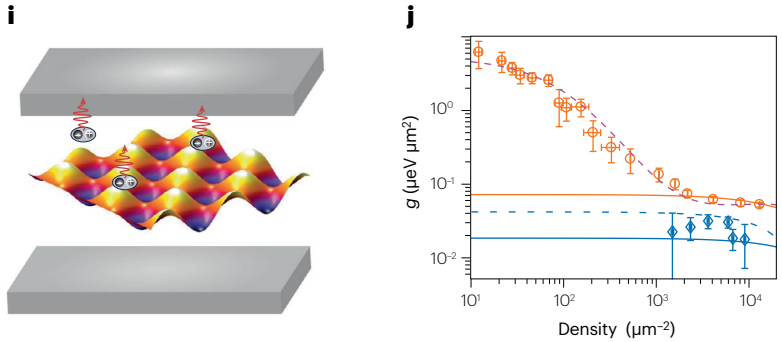

Fig. 4 | Pathways to achieve strong photon nonlinearity through exciton-polaritons. a, Excitation and re-emission of an exciton-polariton by a single photon. Interactions shift the mode off resonance, suppressing multiphoton transmission (known as the polariton blockade). **b**, Detuning-dependent coincidence counts and the corresponding non-classical correlations of polaritons in a quantum-well microcavity. **c**, Absorption in a natural Cu_2O crystal resolving excitonic resonances for large principal quantum numbers. **d**, Formation of Rydberg exciton-polaritons under strong-coupling regime for $n = 3,\ldots, 6$. **e**, Rabi splitting versus exciton density and pump fluence for different principal quantum numbers n, revealing an increase in n-dependent nonlinear coefficient. **f**, A bilayer MoS_2 coupled to a Fabry–Perot microcavity and the possible exciton configurations between layers L_1 and L_2 (with no external field applied). These interlayer excitons have permanent out-of-plane dipoles and strong, long-range interactions. **g**, Polariton dispersion showing multiple coupled excitonic species, showing the polariton eigenvalues (yellow lines) and the exciton and cavity modes (brown lines). **h**, Interlayer (dipolar) polaritons (green) showing enhanced nonlinearity compared with neutral exciton-polaritons (orange), evident in low-density reduction of apparent Rabi splitting. **i**, Moiré polariton system formed by an exciton confined in a moiré lattice, coupled to a cavity. **j**, Nonlinear enhancement of moiré excitons (orange) over intralayer exciton-polaritons (blue). Γ_p, polariton linewidth. Panel **a** reprinted from ref. 289, Springer Nature Limited. Panel **b** reprinted from ref. 210, Springer Nature Limited. Panels **c** and **d** adapted from ref. 290, Springer Nature Limited. Panel **e** reprinted from ref. 222, Springer Nature Limited. Panels **f**–**h** adapted from ref. 228, CC BY 4.0. Panels **i** and **j** reprinted from ref. 229, Springer Nature Limited.

sequence of pulses with an interpulse delay chosen to allow selective coupling with nuclei of particular hyperfine coupling strengths. This protocol leads to relatively long entangling gate times but allows for the possibility of multiqubit entangling gates[253,254], which can perform better – as also shown experimentally[255] – than sequential nuclear spin entangling gates[256]. The latter approach is not well suited for a dense nuclear spin bath, such as in QDs, and performs better with sparse baths in which the number of nuclear spins of a particular hyperfine strength is relatively low, reducing the number of unwanted interactions. Such baths are characteristic of diamond and silicon, which have a natural abundance of nuclear spin isotopes ^{13}C and ^{29}Si, respectively, and the different nuclear spin species can be beneficial both in terms of coherence times[257,258] and gate fidelities[259]. Conditional gates between the defect electronic spin and nearby as well as distant nuclear spin gates have been demonstrated experimentally for N–V centres. However, owing to their small Debye–Waller factor of ~3%, they are not best suited for operation as QEs. By contrast, recent interest has been increasing for defects in silicon, such as T and G centres[260–262], which emit in the telecommunication band, making them optimal for fibre-optic communication. These emitters also show small Debye–Waller factors (approximately 23% and 18%, respectively), but recent experiments have demonstrated improvements when embedded in cavities, for example for T centres[263,264] and G centres[265,266]. By using spin defects as QEs and the surrounding nuclear spins as qubits, the latter can temporarily store the entanglement with already emitted photons, whereas the former generates new parts of the graph state[267]. For example, the presence of a nuclear spin near a solid-state defect emitter suffices to generate resource states for quantum networks[267], and, at the protocol level, a method for the generation of arbitrary photonic graph states has also been developed[268].

Characterization of entanglement structure

Verifying that one has indeed generated the desired cluster or graph state – and characterizing its entanglement structure – is a non-trivial task that generally becomes more challenging as the number of photons increases. The 'gold standard' method is quantum-state tomography, wherein a large set of measurements in different bases is collected to reconstruct the full multiqubit density matrix. Tomography provides complete information, allowing one to compute state fidelity and entanglement measures, and to directly observe the exact structure of entanglement (such as which qubits are pairwise entangled). However, its large measurement overhead makes it impractical in the many-body setting. Instead, specialized measures that leverage the stabilizer structure of graph states can be estimated more efficiently.

Two common strategies to verify entanglement in a state are estimating the fidelity between the experimental state and the desired graph state, and estimating an entanglement witness. For GHZ, graph and cluster states, lower bounds on the fidelity can be efficiently estimated using local measurements of a small set of stabilizer generators[269–272]. Under realistic noise models, the lower bound on the fidelity can be improved substantially while requiring a number of samples that scales only linearly with the number of qubits[273]. The fidelity with an entangled stabilizer state is intimately linked to the verification of entanglement using an entanglement witness W, defined as an operator whose expectation value satisfies $\mathrm{Tr}(W\rho) \geq 0$ for all states that are separable across some bipartition. Thus, if one finds $\mathrm{Tr}(W\rho) < 0$, the state ρ exhibits genuine multipartite entanglement. The expectation value can be estimated using the same stabilizer measurements as used for the fidelity lower bound, so no extra overhead is incurred. This kind of entanglement witness has been used to certify the multipartite entanglement in 14-photon GHZ states and 12-photon linear cluster states[242].

Although these strategies provide a lower bound on the fidelity, this bound is not necessarily tight. Instead, one might want to estimate the infidelity to a desired precision with high confidence. Such an estimate can be achieved through random sequences of local Pauli measurements[274,275]. The number of sequences is independent on the size of the system and depends only weakly on the precision and confidence.

Outlook and future perspectives

Many-body entanglement in emitter arrays and their emitted photons constitute a fundamental resource for all three main quantum technologies: quantum computation, communication and sensing (Fig. 5g–i). In sensing applications (Fig. 5g), twin Fock states[276,277] and N00N states[278,279] have long been known to be optimal for phase estimation, as measured by the Heisenberg scaling of the estimation mean-squared error (N00N states are also commonly known as GHZ states in quantum information theory literature)[244,280]. Photonic states generated in superradiant bursts in both waveguide QED and cavity QED systems can also achieve Heisenberg scaling[89,126] (Fig. 5g). A key advantage of this approach is that, unlike graph-state generation, producing superradiant bursts does not require full coherent control over the QEs[129,172–174,176,177,281] and thus may be more straightforward to realize in solid-state QEs. However, the direct usefulness of the superradiant states to quantum sensing remains an open problem. In particular, the impact of experimental non-idealities, such as emitter inhomogeneities, photon loss and dephasing, on the metrological potential of the superradiantly emitted photons remains to be understood. Moreover,

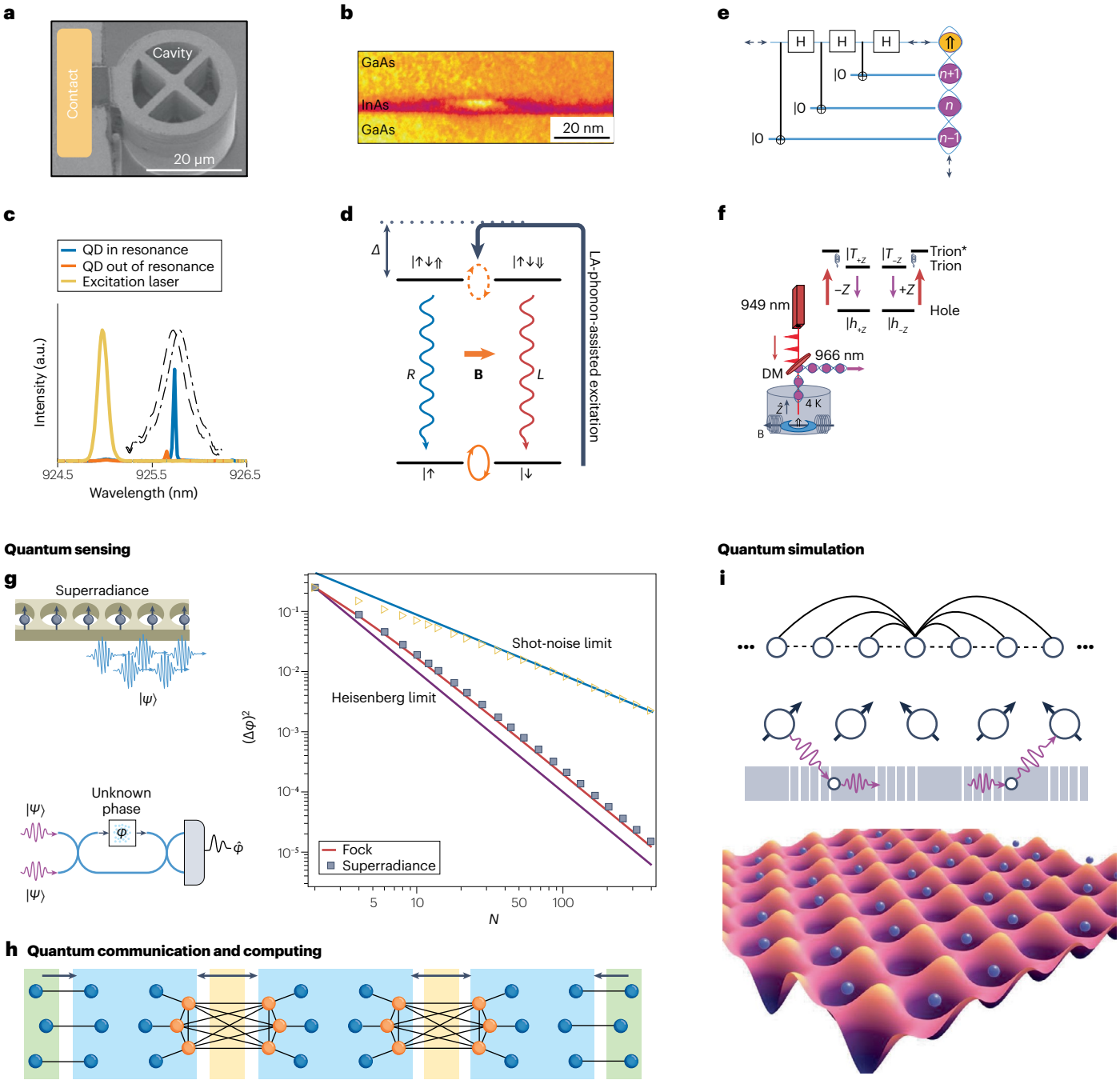

optimal measurement protocols that actually attain the Heisenberg limit with such states need to be identified. The optimal measurement scheme would require either the generation of optical nonlinearities, as theoretically proposed[89], or a case-by-case development of simple observables (such as an optical analogue of spin squeezing parameter) that can be easily measured.

For optical quantum computing (Fig. 5h), the state-of-the-art strategy involves generating specific cluster states which are computationally universal. This universality means that, given this resource state, a quantum circuit can be effectively implemented with a specific sequence of measurements and feedback[236,282]. Furthermore, fusion-based quantum computation has been introduced in recent proposals[283], where constant-size, independent of the target algorithm, graph states (such as four-ring or six-ring graphs) are generated and consumed as an elementary resource for computation. However, building an end-to-end quantum computation scheme with QEs, especially while also using fusion measurements, requires high photon indistinguishability for high fidelities. Correlated errors are an unavoidable

Fig. 5 | Generation of graph states and applications of many-body entanglement. a–**d**, Quantum-dot (QD) platforms for cluster and graph-state generation. Negatively charged QD in the centre of a connected pillar optical cavity (panel **a**); single InGaAs QD with GaAs barriers (panel **b**); representative QD emission spectrum obtained through reflectivity measurements (black dashed lines) (panel **c**); energy levels and optical selection rules of a negatively charged QD in the presence of a small (<100 mT) transverse magnetic field (panel **d**). Blue-detuned excitation enables phonon-assisted excitation by longitudinal acoustic (LA) phonons. **e**–**h**, Deterministic cluster-state generation. Cluster-state generation using sequential Hadamard and CNOT gates (panel **e**); experimental set-up for QD-based cluster-state generation with a dichroic mirror (DM) and magnetic field along the *x* axis, where the states refer to the hole, trion and excited trion states (panel **f**); applications of many-body entangled states: quantum-enhanced phase sensing[280] (top left); superradiant emission surpassing shot-noise limit (right); graph states generated by specialized quantum emitters, such as QDs, as resource states for quantum communication and quantum computation (bottom left) (panel **g**). Panel **h** shows the protocol for a quantum repeater to establish entanglement between two observers (green blocks) via a series of repeater nodes (blue blocks) and source nodes (yellow blocks). Repeater graphs are shown with core (orange circles) and arm (blue circles) nodes, where the connecting black lines denote entanglement. **i**, Long-range qubit interactions enabling quantum simulation of complex many-body systems. Panels **a**–**d** reprinted from ref. 8, Springer Nature Limited. Panels **e** and **f** reprinted from ref. 7, Springer Nature Limited. Panel **g** right image adapted with permission from ref. 126, APS. Panel **h** adapted from ref. 291, CC BY 4.0.

part of photonic graph-state generation, as a single QE error can propagate to some of the emitted photons following the error. The correlation time is given by the duration between two measurements of the QE state during the graph-state generation protocol. Although the impact of various sources of noise has been considered for fault-tolerance quantum computation with cluster states[284–286], a current focus of ongoing research is to understand how fault tolerance can be maintained under temporally correlated noise.

Graph states have also found important utility in all-photonic quantum networks[287]. This application relies on generating repeater graph states at source nodes before distributing them to intermediate nodes and performing entanglement swapping. Therefore, similarly to fusion-based quantum computation, this application also requires high photon indistinguishability. The generation of repeater graph states with a minimal number of QEs has been discussed elsewhere[268]. When working with quantum defects in solids, an alternative is to use a single QE and multiple nuclear spins that can be addressed using the defect spin[267]. Improvements in the Debye–Waller factor and advancements in the nuclear spin control pulses for these defects will be important milestones in the generation of repeater-type graph states. Solid-state emitters are additionally well suited for applications in one-way quantum repeaters[288].

Finally, in addition to being used as light sources, QEs coupled to nanophotonic structures can also be a testbed for simulating many-body physics[136,137] (Fig. 5i). The ability to tune the electromagnetic Green's function with nanophotonic structures opens up the possibility of engineering long-range coherent and dissipative interaction between QEs (Box 2). These systems could thus potentially be used as quantum simulators for studying the physics of all-to-all models that arise routinely in quantum optics, condensed matter physics and quantum chemistry.

To realize these potential applications in quantum sensing, computation, communication and simulation, further advances in solid-state QEs are essential. For more established platforms such as self-assembled III–V quantum dots, colour centres in diamond, and DBT molecules in organic crystals, the next key step is to scale coherent control beyond the few-emitter limit. Nanophotonic integration, emitter tuning, active stabilization against spectral diffusion, and high-efficiency collection offer routes to achieving this control. For emitters hosted in 2D materials, parallel progress must come from improved material growth and a deeper microscopic understanding of coherence. In TMDs and their heterostructures, strong exciton–exciton interactions and moiré engineering make this platform especially promising for optical nonlinearities, but pushing towards the single-photon nonlinearity regime will require higher cooperativity and longer exciton coherence. In hBN, the open challenge is to achieve simultaneous spin and optical coherence so that a single defect can serve as both a high-quality spin qubit and a source of indistinguishable photons for entanglement generation. For colloidal QDs, encouraging demonstrations of many-body coherence in large ensembles have emerged, but deterministic integration with nanophotonics and individual emitter control are still at an earlier stage of development. Meeting these targets would unlock many-body entanglement from large QE arrays in the solid state, with direct impact on quantum technologies.

Published online: 17 February 2026

References

1. Kimble, H. J. The quantum internet. *Nature* **453**, 1023–1030 (2008).
2. Lodahl, P. Scaling up solid-state quantum photonics. *Science* **362**, 646–647 (2018).
3. Turunen, M. et al. Quantum photonics with layered 2D materials. *Nat. Rev. Phys.* **4**, 219–236 (2022).
4. Heinrich, A. J. et al. Quantum-coherent nanoscience. *Nat. Nanotechnol.* **16**, 1318–1329 (2021).
5. Evans, R. E. et al. Photon-mediated interactions between quantum emitters in a diamond nanocavity. *Science* **362**, 662–665 (2018).
6. Dousse, A. et al. Ultrabright source of entangled photon pairs. *Nature* **466**, 217–220 (2010).
7. Cogan, D., Su, Z.-E., Kenneth, O. & Gershoni, D. Deterministic generation of indistinguishable photons in a cluster state. *Nat. Photon.* **17**, 324–329 (2023).
8. Coste, N. et al. High-rate entanglement between a semiconductor spin and indistinguishable photons. *Nat. Photon.* **17**, 582–587 (2023).
9. Grim, J. Q. et al. Scalable in operando strain tuning in nanophotonic waveguides enabling three-quantum-dot superradiance. *Nat. Mater.* **18**, 963–969 (2019).
10. Atatüre, M., Englund, D., Vamivakas, A. N., Lee, S.-Y. & Wrachtrup, J. Material platforms for spin-based photonic quantum technologies. *Nat. Rev. Mater.* **3**, 38–51 (2018).
11. Senellart, P., Solomon, G. & White, A. High-performance semiconductor quantum-dot single-photon sources. *Nat. Nanotechnol.* **12**, 1026–1039 (2017).
12. Awschalom, D. D., Hanson, R., Wrachtrup, J. & Zhou, B. B. Quantum technologies with optically interfaced solid-state spins. *Nat. Photon.* **12**, 516–527 (2018).
13. O'Brien, J. L., Furusawa, A. & Vučković, J. Photonic quantum technologies. *Nat. Photon.* **3**, 687–695 (2009).
14. He, Y.-M. et al. Single quantum emitters in monolayer semiconductors. *Nat. Nanotechnol.* **10**, 497–502 (2015).
15. Tomm, N. et al. A bright and fast source of coherent single photons. *Nat. Nanotechnol.* **16**, 399–403 (2021).
16. Toninelli, C. et al. Single organic molecules for photonic quantum technologies. *Nat. Mater.* **20**, 1615–1628 (2021).
17. Aharonovich, I., Tetienne, J.-P. & Toth, M. Quantum emitters in hexagonal boron nitride. *Nano Lett.* **22**, 9227–9235 (2022).
18. Zhai, L. et al. Low-noise GaAs quantum dots for quantum photonics. *Nat. Commun.* **11**, 4745 (2020).
19. Gurioli, M., Wang, Z., Rastelli, A., Kuroda, T. & Sanguinetti, S. Droplet epitaxy of semiconductor nanostructures for quantum photonic devices. *Nat. Mater.* **18**, 799–810 (2019).
20. Uppu, R., Midolo, L., Zhou, X., Carolan, J. & Lodahl, P. Quantum-dot-based deterministic photon-emitter interfaces for scalable photonic quantum technology. *Nat. Nanotechnol.* **16**, 1308–1317 (2021).
21. Gao, X. et al. Single nuclear spin detection and control in a van der Waals material. *Nature* **643**, 943–949 (2025).

22. Li, X. et al. Proximity-induced chiral quantum light generation in strain-engineered $WSe_2/NiPS_3$ heterostructures. *Nat. Mater.* **22**, 1311–1316 (2023).
23. Senichev, A. et al. Room-temperature single-photon emitters in silicon nitride. *Sci. Adv.* **7**, eabj0627 (2021).
24. González-Tudela, A., Reiserer, A., García-Ripoll, J. J. & García-Vidal, F. J. Light–matter interactions in quantum nanophotonic devices. *Nat. Rev. Phys.* **6**, 166–179 (2024).
25. Molesky, S. et al. Inverse design in nanophotonics. *Nat. Photon.* **12**, 659–670 (2018).
26. Rodt, S. & Reitzenstein, S. Integrated nanophotonics for the development of fully functional quantum circuits based on on-demand single-photon emitters. *APL Photonics* **6**, 010901 (2021).
27. Lukin, D. M., Guidry, M. A. & Vučković, J. Integrated quantum photonics with silicon carbide: challenges and prospects. *PRX Quantum* **1**, 020102 (2020).
28. Wang, J., Sciarrino, F., Laing, A. & Thompson, M. G. Integrated photonic quantum technologies. *Nat. Photon.* **14**, 273–284 (2020).
29. Pelucchi, E. et al. The potential and global outlook of integrated photonics for quantum technologies. *Nat. Rev. Phys.* **4**, 194–208 (2022).
30. Senichev, A. et al. Quantum emitters in aluminum nitride induced by heavy ion irradiation. *APL Quantum* **1**, 036103 (2024).
31. Aharonovich, I., Englund, D. & Toth, M. Solid-state single-photon emitters. *Nat. Photon.* **10**, 631–641 (2016).
32. Fox, A. M. Solid-state quantum emitters. *Adv. Quantum Technol.* **8**, 2300390 (2025).
33. Chen, J. et al. Low-dimensional solid-state single-photon emitters. *Nanophotonics* **14**, 1687–1713 (2025).
34. Zuber, J. A. et al. Shallow silicon vacancy centers with lifetime-limited optical linewidths in diamond nanostructures. *Nano Lett.* **23**, 10901–10907 (2023).
35. Sipahigil, A. et al. Indistinguishable photons from separated silicon-vacancy centers in diamond. *Phys. Rev. Lett.* **113**, 113602 (2014).
36. Pedersen, F. T. et al. Near transform-limited quantum dot linewidths in a broadband photonic crystal waveguide. *ACS Photonics* **7**, 2343–2349 (2020).
37. Thyrrestrup, H. et al. Quantum optics with near-lifetime-limited quantum-dot transitions in a nanophotonic waveguide. *Nano Lett.* **18**, 1801–1806 (2018).
38. Santori, C., Fattal, D., Vučković, J., Solomon, G. S. & Yamamoto, Y. Indistinguishable photons from a single-photon device. *Nature* **419**, 594–597 (2002).
39. Lombardi, P. et al. Triggered emission of indistinguishable photons from an organic dye molecule. *Appl. Phys. Lett.* **118**, 204002 (2021).
40. Kuhlmann, A. V. et al. Transform-limited single photons from a single quantum dot. *Nat. Commun.* **6**, 8204 (2015).
41. Kuhlmann, A. V. et al. Charge noise and spin noise in a semiconductor quantum device. *Nat. Phys.* **9**, 570–575 (2013).
42. Çakan, A. et al. Quantum optics applications of hexagonal boron nitride defects. *Adv. Opt. Mater.* **13**, 2402508 (2025).
43. Toth, M. & Aharonovich, I. Single photon sources in atomically thin materials. *Annu. Rev. Phys. Chem.* **70**, 123–142 (2019).
44. Gao, T., von Helversen, M., Antón-Solanas, C., Schneider, C. & Heindel, T. Atomically-thin single-photon sources for quantum communication. *npj 2D Mater. Appl.* **7**, 4 (2023).
45. Zotev, P. G. et al. Nanophotonics with multilayer van der Waals materials. *Nat. Photon.* **19**, 788–802 (2025).
46. Esmann, M., Wein, S. C. & Antón-Solanas, C. Solid-state single-photon sources: recent advances for novel quantum materials. *Adv. Funct. Mater.* **34**, 2315936 (2024).
47. Castelletto, S., Inam, F. A., Sato, S.-I. & Boretti, A. Hexagonal boron nitride: a review of the emerging material platform for single-photon sources and the spin–photon interface. *Beilstein J. Nanotechnol.* **11**, 740–769 (2020).
48. Shaik, A. B. & Palla, P. Optical quantum technologies with hexagonal boron nitride single photon sources. *Sci. Rep.* **11**, 12285 (2021).
49. Dietrich, A. et al. Observation of Fourier transform limited lines in hexagonal boron nitride. *Phys. Rev. B* **98**, 081414 (2018).
50. Kianinia, M., Xu, Z.-Q., Toth, M. & Aharonovich, I. Quantum emitters in 2D materials: emitter engineering, photophysics, and integration in photonic nanostructures. *Appl. Phys. Rev.* **9**, 011306 (2022).
51. Fournier, C. et al. Two-photon interference from a quantum emitter in hexagonal boron nitride. *Phys. Rev. Appl.* **19**, L041003 (2023).
52. Akbari, H. et al. Lifetime-limited and tunable quantum light emission in h-BN via electric field modulation. *Nano Lett.* **22**, 7798–7803 (2022).
53. Ding, X. et al. On-demand single photons with high extraction efficiency and near-unity indistinguishability from a resonantly driven quantum dot in a micropillar. *Phys. Rev. Lett.* **116**, 020401 (2016).
54. Somaschi, N. et al. Near-optimal single-photon sources in the solid state. *Nat. Photon.* **10**, 340–345 (2016).
55. Bar-Gill, N., Pham, L. M., Jarmola, A., Budker, D. & Walsworth, R. L. Solid-state electronic spin coherence time approaching one second. *Nat. Commun.* **4**, 1743 (2013).
56. Hepp, C. et al. Electronic structure of the silicon vacancy color center in diamond. *Phys. Rev. Lett.* **112**, 036405 (2014).
57. Pingault, B. et al. Coherent control of the silicon-vacancy spin in diamond. *Nat. Commun.* **8**, 15579 (2017).
58. Rogers, L. J. et al. All-optical initialization, readout, and coherent preparation of single silicon-vacancy spins in diamond. *Phys. Rev. Lett.* **113**, 263602 (2014).
59. Vaidya, S., Gao, X., Dikshit, S., Aharonovich, I. & Li, T. Quantum sensing and imaging with spin defects in hexagonal boron nitride. *Adv. Phys. X* **8**, 2206049 (2023).
60. Gong, R. et al. Coherent dynamics of strongly interacting electronic spin defects in hexagonal boron nitride. *Nat. Commun.* **14**, 3299 (2023).
61. Xu, X. et al. Greatly enhanced emission from spin defects in hexagonal boron nitride enabled by a low-loss plasmonic nanocavity. *Nano Lett.* **23**, 25–33 (2023).
62. Haykal, A. et al. Decoherence of V_B^- spin defects in monoisotopic hexagonal boron nitride. *Nat. Commun.* **13**, 4347 (2022).
63. Rizzato, R. et al. Extending the coherence of spin defects in hBN enables advanced qubit control and quantum sensing. *Nat. Commun.* **14**, 5089 (2023).
64. Cywiński, Ł, Witzel, W. M. & Das Sarma, S. Pure quantum dephasing of a solid-state electron spin qubit in a large nuclear spin bath coupled by long-range hyperfine-mediated interactions. *Phys. Rev. B* **79**, 245314 (2009).
65. Gillard, G., Clarke, E. & Chekhovich, E. A. Harnessing many-body spin environment for long coherence storage and high-fidelity single-shot qubit readout. *Nat. Commun.* **13**, 4048 (2022).
66. Nguyen, G. N. et al. Enhanced electron-spin coherence in a GaAs quantum emitter. *Phys. Rev. Lett.* **131**, 210805 (2023).
67. Vannucci, L. & Gregersen, N. Highly efficient and indistinguishable single-photon sources via phonon-decoupled two-color excitation. *Phys. Rev. B* **107**, 195306 (2023).
68. Kuruma, K. et al. Controlling interactions between high-frequency phonons and single quantum systems using phononic crystals. *Nat. Phys.* **21**, 77–82 (2025).
69. MacCabe, G. S. et al. Nano-acoustic resonator with ultralong phonon lifetime. *Science* **370**, 840–843 (2020).
70. Meesala, S. et al. Strain engineering of the silicon-vacancy center in diamond. *Phys. Rev. B* **97**, 205444 (2018).
71. Ramsay, A. J. et al. Coherence protection of spin qubits in hexagonal boron nitride. *Nat. Commun.* **14**, 461 (2023).
72. Sohn, Y.-I. et al. Controlling the coherence of a diamond spin qubit through its strain environment. *Nat. Commun.* **9**, 2012 (2018).
73. Rosenthal, E. I. et al. Single-shot readout and weak measurement of a tin-vacancy qubit in diamond. *Phys. Rev. X* **14**, 041008 (2024).
74. Finley, J. J. et al. Quantum-confined Stark shifts of charged exciton complexes in quantum dots. *Phys. Rev. B* **70**, 201308 (2004).
75. Gerardot, B. D. et al. Manipulating exciton fine structure in quantum dots with a lateral electric field. *Appl. Phys. Lett.* **90**, 041101 (2007).
76. Höfer, B. et al. Tuning emission energy and fine structure splitting in quantum dots emitting in the telecom O-band. *AIP Adv.* **9**, 085112 (2019).
77. Luo, J.-W., Singh, R., Zunger, A. & Bester, G. Influence of the atomic-scale structure on the exciton fine-structure splitting in InGaAs and GaAs quantum dots in a vertical electric field. *Phys. Rev. B* **86**, 161302 (2012).
78. Colautti, M. et al. Laser-induced frequency tuning of Fourier-limited single-molecule emitters. *ACS Nano* **14**, 13584–13592 (2020).
79. Duquennoy, R. et al. Enhanced control of single-molecule emission frequency and spectral diffusion. *ACS Nano* **18**, 32508–32516 (2024).
80. Zheng, S.-B. & Guo, G.-C. Efficient scheme for two-atom entanglement and quantum information processing in cavity QED. *Phys. Rev. Lett.* **85**, 2392–2395 (2000).
81. Majer, J. et al. Coupling superconducting qubits via a cavity bus. *Nature* **449**, 443–447 (2007).
82. Lange, C. M., Daggett, E., Walther, V., Huang, L. & Hood, J. D. Superradiant and subradiant states in lifetime-limited organic molecules through laser-induced tuning. *Nat. Phys.* **20**, 836–842 (2024).
83. Day, M. W. et al. Coherent interactions between silicon-vacancy centers in diamond. *Phys. Rev. Lett.* **128**, 203603 (2022).
84. Tiranov, A. et al. Collective super- and subradiant dynamics between distant optical quantum emitters. *Science* **379**, 389–393 (2023).
85. Trebbia, J.-B., Deplano, Q., Tamarat, P. & Lounis, B. Tailoring the superradiant and subradiant nature of two coherently coupled quantum emitters. *Nat. Commun.* **13**, 2962 (2022).
86. González-Tudela, A., Paulisch, V., Chang, D. E., Kimble, H. J. & Cirac, J. I. Deterministic generation of arbitrary photonic states assisted by dissipation. *Phys. Rev. Lett.* **115**, 163603 (2015).
87. González-Tudela, A., Paulisch, V., Kimble, H. J. & Cirac, J. I. Efficient multiphoton generation in waveguide quantum electrodynamics. *Phys. Rev. Lett.* **118**, 213601 (2017).
88. Rubies-Bigorda, O., Masson, S. J., Yelin, S. F. & Asenjo-Garcia, A. Deterministic generation of photonic entangled states using decoherence-free subspaces. *Phys. Rev. Lett.* **134**, 213603 (2025).
89. Abbasgholinejad, E., Malz, D., Asenjo-Garcia, A. & Trivedi, R. Theory of quantum-enhanced interferometry with general Markovian light sources. Preprint at https://doi.org/10.48550/arXiv.2504.05111 (2025).
90. Lukin, D. M. et al. Two-emitter multimode cavity quantum electrodynamics in thin-film silicon carbide photonics. *Phys. Rev. X* **13**, 011005 (2023).
91. Lukin, D. M. et al. Mesoscopic cavity quantum electrodynamics with phase-disordered emitters in a Kerr nonlinear resonator. Preprint at https://doi.org/10.48550/arXiv.2504.09324 (2025).
92. Fano, U. Description of states in quantum mechanics by density matrix and operator techniques. *Rev. Mod. Phys.* **29**, 74 (1957).
93. Wootters, W. K. & Fields, B. D. Optimal state-determination by mutually unbiased measurements. *Ann. Phys.* **191**, 363–381 (1989).
94. Elben, A. et al. The randomized measurement toolbox. *Nat. Rev. Phys.* **5**, 9–24 (2023).

95. Elben, A. et al. Mixed-state entanglement from local randomized measurements. *Phys. Rev. Lett.* **125**, 200501 (2020).
96. Vermersch, B. et al. Many-body entropies and entanglement from polynomially many local measurements. *Phys. Rev. X* **14**, 031035 (2024).
97. Huang, H.-Y., Kueng, R. & Preskill, J. Predicting many properties of a quantum system from very few measurements. *Nat. Phys.* **16**, 1050–1057 (2020).
98. Chuang, I. L. & Nielsen, M. A. Prescription for experimental determination of the dynamics of a quantum black box. *J. Mod. Opt.* **44**, 2455–2467 (1997).
99. Mohseni, M., Rezakhani, A. T. & Lidar, D. A. Quantum-process tomography: resource analysis of different strategies. *Phys. Rev. A* **77**, 032322 (2008).
100. Haah, J., Hunter-Jones, N., Liu, Y., Tran, M. C. & Xu, S. Learning quantum Hamiltonians from high-temperature Gibbs states and real-time evolutions. *Nat. Phys.* **20**, 370–376 (2023).
101. Stick-Franca, D., Roth, I. & Eisert, J. Efficient and robust estimation of many-qubit Hamiltonians. *Nat. Commun.* **15**, 963 (2023).
102. Auffèves, A., Gerace, D., Portolan, S., Drezet, A. & França Santos, M. Few emitters in a cavity: from cooperative emission to individualization. *New J. Phys.* **13**, 093020 (2011).
103. Bhatti, D., Von Zanthier, J. & Agarwal, G. S. Superbunching and nonclassicality as new hallmarks of superradiance. *Sci. Rep.* **5**, 17335 (2015).
104. Koong, Z. X. et al. Coherence in cooperative photon emission from indistinguishable quantum emitters. *Sci. Adv.* **8**, eabm8171 (2022).
105. Machielse, B. et al. Quantum interference of electromechanically stabilized emitters in nanophotonic devices. *Phys. Rev. X* **9**, 031022 (2019).
106. Kim, J., Aghaeimeibodi, S., Richardson, C. J., Leavitt, R. P. & Waks, E. Super-radiant emission from quantum dots in a nanophotonic waveguide. *Nano Lett.* **18**, 4734–4740 (2018).
107. Sipahigil, A. et al. An integrated diamond nanophotonics platform for quantum-optical networks. *Science* **354**, 847–850 (2016).
108. Cygorek, M. et al. Signatures of cooperative emission in photon coincidence: superradiance versus measurement-induced cooperativity. *Phys. Rev. A* **107**, 023718 (2023).
109. Flagg, E. B. et al. Interference of single photons from two separate semiconductor quantum dots. *Phys. Rev. Lett.* **104**, 137401 (2010).
110. Patel, R. B. et al. Two-photon interference of the emission from electrically tunable remote quantum dots. *Nat. Photon.* **4**, 632–635 (2010).
111. Bohr, E. A. et al. Collectively enhanced Ramsey readout by cavity sub- to superradiant transition. *Nat. Commun.* **15**, 1084 (2024).
112. Hotter, C., Ostermann, L. & Ritsch, H. Cavity sub- and superradiance for transversely driven atomic ensembles. *Phys. Rev. Res.* **5**, 013056 (2023).
113. Dicke, R. H. Coherence in spontaneous radiation processes. *Phys. Rev.* **93**, 99–110 (1954).
114. Gross, M. & Haroche, S. Superradiance: an essay on the theory of collective spontaneous emission. *Phys. Rep.* **93**, 301–396 (1982).
115. Masson, S. J. & Asenjo-Garcia, A. Universality of Dicke superradiance in arrays of quantum emitters. *Nat. Commun.* **13**, 2285 (2022).
116. Masson, S. J., Covey, J. P., Will, S. & Asenjo-Garcia, A. Dicke superradiance in ordered arrays of multilevel atoms. *PRX Quantum* **5**, 010344 (2024).
117. Sierra, E., Masson, S. J. & Asenjo-Garcia, A. Dicke superradiance in ordered lattices: dimensionality matters. *Phys. Rev. Res.* **4**, 023207 (2022).
118. Cardenas-Lopez, S., Masson, S. J., Zager, Z. & Asenjo-Garcia, A. Many-body superradiance and dynamical mirror symmetry breaking in waveguide QED. *Phys. Rev. Lett.* **131**, 033605 (2023).
119. Masson, S. J., Ferrier-Barbut, I., Orozco, L. A., Browaeys, A. & Asenjo-Garcia, A. Many-body signatures of collective decay in atomic chains. *Phys. Rev. Lett.* **125**, 263601 (2020).
120. Robicheaux, F. Theoretical study of early-time superradiance for atom clouds and arrays. *Phys. Rev. A* **104**, 063706 (2021).
121. Rainò, G. et al. Superfluorescence from lead halide perovskite quantum dot superlattices. *Nature* **563**, 671–675 (2018).
122. Blach, D. D. et al. Superradiance and exciton delocalization in perovskite quantum dot superlattices. *Nano Lett.* **22**, 7811–7818 (2022).
123. Luo, L. et al. Polarized superradiance from $CsPbBr_3$ quantum dot superlattice with controlled interdot electronic coupling. *Nano Lett.* **25**, 6176–6183 (2025).
124. Rainò, G., Utzat, H., Bawendi, M. G. & Kovalenko, M. V. Superradiant emission from self-assembled light emitters: from molecules to quantum dots. *MRS Bull.* **45**, 841–848 (2020).
125. Kumlin, J. Superradiance of strongly interacting dipolar excitons in moiré quantum materials. *Phys. Rev. Lett.* **134**, 126901 (2025).
126. Paulisch, V., Perarnau-Llobet, M., González-Tudela, A. & Cirac, J. I. Quantum metrology with one-dimensional superradiant photonic states. *Phys. Rev. A* **99**, 043807 (2019).
127. Lei, M. et al. Many-body cavity quantum electrodynamics with driven inhomogeneous emitters. *Nature* **617**, 271–276 (2023).
128. Li, X., Marino, J., Chang, D. E. & Flebus, B. Solid-state platform for cooperative quantum dynamics driven by correlated emission. *Phys. Rev. B* **111**, 064424 (2025).
129. Asenjo-Garcia, A., Moreno-Cardoner, M., Albrecht, A., Kimble, H. J. & Chang, D. E. Exponential improvement in photon storage fidelities using subradiance and 'selective radiance' in atomic arrays. *Phys. Rev. X* **7**, 031024 (2017).
130. Gorshkov, A. V., André, A., Fleischhauer, M., Sørensen, A. S. & Lukin, M. D. Universal approach to optimal photon storage in atomic media. *Phys. Rev. Lett.* **98**, 123601 (2007).
131. Mishra, S. D., Trivedi, R., Safavi-Naeini, A. H. & Vučković, J. Control design for inhomogeneous-broadening compensation in single-photon transducers. *Phys. Rev. Appl.* **16**, 044025 (2021).
132. Zanardi, P. & Rasetti, M. Error avoiding quantum codes. *Mod. Phys. Lett. B* **11**, 1085–1093 (1997).
133. Lidar, D. A., Chuang, I. L. & Whaley, K. B. Decoherence-free subspaces for quantum computation. *Phys. Rev. Lett.* **81**, 2594–2597 (1998).
134. Beige, A., Braun, D., Tregenna, B. & Knight, P. L. Quantum computing using dissipation to remain in a decoherence-free subspace. *Phys. Rev. Lett.* **85**, 1762–1765 (2000).
135. Beige, A., Braun, D. & Knight, P. L. Driving atoms into decoherence-free states. *New J. Phys.* **2**, 22 (2000).
136. Kennes, D. M. et al. Moiré heterostructures as a condensed-matter quantum simulator. *Nat. Phys.* **17**, 155–163 (2021).
137. Noh, C. & Angelakis, D. G. Quantum simulations and many-body physics with light. *Rep. Prog. Phys.* **80**, 016401 (2016).
138. Mak, K. F. & Shan, J. Semiconductor moiré materials. *Nat. Nanotechnol.* **17**, 686–695 (2022).
139. Götting, N., Lohof, F. & Gies, C. Moiré-Bose-Hubbard model for interlayer excitons in twisted transition metal dichalcogenide heterostructures. *Phys. Rev. B* **105**, 165419 (2022).
140. Baek, H. et al. Highly energy-tunable quantum light from moiré-trapped excitons. *Sci. Adv.* **6**, eaba8526 (2020).
141. Jin, C. et al. Observation of moiré excitons in WSe_2/WS_2 heterostructure superlattices. *Nature* **567**, 76–80 (2019).
142. Marti, S. et al. Quantum squeezing in a nonlinear mechanical oscillator. *Nat. Phys.* **20**, 1448–1453 (2024).
143. Deng, S. et al. Frozen non-equilibrium dynamics of exciton Mott insulators in moiré superlattices. *Nat. Mater.* **24**, 527–534 (2025).
144. Gross, C. & Bloch, I. Quantum simulations with ultracold atoms in optical lattices. *Science* **357**, 995–1001 (2017).
145. Lodahl, P., Mahmoodian, S. & Stobbe, S. Interfacing single photons and single quantum dots with photonic nanostructures. *Rev. Mod. Phys.* **87**, 347–400 (2015).
146. Bradac, C., Gao, W., Forneris, J., Trusheim, M. E. & Aharonovich, I. Quantum nanophotonics with group IV defects in diamond. *Nat. Commun.* **10**, 5625 (2019).
147. Wang, D. et al. Turning a molecule into a coherent two-level quantum system. *Nat. Phys.* **15**, 483–489 (2019).
148. Uppu, R. et al. Scalable integrated single-photon source. *Sci. Adv.* **6**, eabc8268 (2020).
149. Arcari, M. et al. Near-unity coupling efficiency of a quantum emitter to a photonic crystal waveguide. *Phys. Rev. Lett.* **113**, 093603 (2014).
150. Komza, L. et al. Multiplexed color centers in a silicon photonic cavity array. *Optica* **12**, 1400–1405 (2025).
151. Yoshie, T. et al. Vacuum Rabi splitting with a single quantum dot in a photonic crystal nanocavity. *Nature* **432**, 200–203 (2004).
152. Hennessy, K. et al. Quantum nature of a strongly coupled single quantum dot–cavity system. *Nature* **445**, 896–899 (2007).
153. Pscherer, A. et al. Single-molecule vacuum Rabi splitting: four-wave mixing and optical switching at the single-photon level. *Phys. Rev. Lett.* **127**, 133603 (2021).
154. Vivas-Viaña, A., Martín-Cano, D. & Muñoz, C. S. Dissipative stabilization of maximal entanglement between non-identical emitters via two-photon excitation. *Phys. Rev. Res.* **6**, 043051 (2024).
155. Ji, X., Roberts, S., Corato-Zanarella, M. & Lipson, M. Methods to achieve ultra-high quality factor silicon nitride resonators. *APL Photonics* **6**, 071101 (2021).
156. Puckett, M. W. et al. 422 Million intrinsic quality factor planar integrated all-waveguide resonator with sub-MHz linewidth. *Nat. Commun.* **12**, 934 (2021).
157. Luke, K., Dutt, A., Poitras, C. B. & Lipson, M. Overcoming Si_3N_4 film stress limitations for high quality factor ring resonators. *Opt. Express* **21**, 22829–22833 (2013).
158. Hosseini, E. S., Yegnanarayanan, S., Atabaki, A. H., Soltani, M. & Adibi, A. High quality planar silicon nitride microdisk resonators for integrated photonics in the visiblewavelength range. *Opt. Express* **17**, 14543–14551 (2009).
159. Ding, S. W. et al. High-Q cavity interface for color centers in thin film diamond. *Nat. Commun.* **15**, 6358 (2024).
160. Vlasov, Y. A., O'boyle, M., Hamann, H. F. & McNab, S. J. Active control of slow light on a chip with photonic crystal waveguides. *Nature* **438**, 65–69 (2005).
161. Lodahl, P. et al. Chiral quantum optics. *Nature* **541**, 473–480 (2017).
162. Söllner, I. et al. Deterministic photon–emitter coupling in chiral photonic circuits. *Nat. Nanotechnol.* **10**, 775–778 (2015).
163. Gramotnev, D. K. & Bozhevolnyi, S. I. Plasmonics beyond the diffraction limit. *Nat. Photon.* **4**, 83–91 (2010).
164. Akselrod, G. M. et al. Probing the mechanisms of large Purcell enhancement in plasmonic nanoantennas. *Nat. Photon.* **8**, 835–840 (2014).
165. Bogdanov, S. I. et al. Ultrabright room-temperature sub-nanosecond emission from single nitrogen-vacancy centers coupled to nanopatch antennas. *Nano Lett.* **18**, 4837–4844 (2018).
166. Ng, C. et al. Plasmonic near-complete optical absorption and its applications. *Adv. Opt. Mater.* **7**, 1801660 (2019).
167. Andersen, S. K. H. et al. Hybrid plasmonic bullseye antennas for efficient photon collection. *ACS Photonics* **5**, 692–698 (2018).
168. Kocoj, C. A. et al. Ultrafast plasmon dynamics of low-loss sodium metasurfaces. *ACS Nano* **19**, 27310–27317 (2025).

169. Gao, Z. et al. Low-loss plasmonics with nanostructured potassium and sodium–potassium liquid alloys. *Nano Lett.* **23**, 7150–7156 (2023).
170. Choi, H., Heuck, M. & Englund, D. Self-similar nanocavity design with ultrasmall mode volume for single-photon nonlinearities. *Phys. Rev. Lett.* **118**, 223605 (2017).
171. Albrechtsen, M. et al. Nanometer-scale photon confinement in topology-optimized dielectric cavities. *Nat. Commun.* **13**, 6281 (2022).
172. Sheremet, A. S., Petrov, M. I., Iorsh, I. V., Poshakinskiy, A. V. & Poddubny, A. N. Waveguide quantum electrodynamics: collective radiance and photon–photon correlations. *Rev. Mod. Phys.* **95**, 015002 (2023).
173. Guerin, W., Araújo, M. O. & Kaiser, R. Subradiance in a large cloud of cold atoms. *Phys. Rev. Lett.* **116**, 083601 (2016).
174. Das, D., Lemberger, B. & Yavuz, D. D. Subradiance and superradiance-to-subradiance transition in dilute atomic clouds. *Phys. Rev. A* **102**, 043708 (2020).
175. Otten, M. et al. Entanglement of two, three, or four plasmonically coupled quantum dots. *Phys. Rev. B* **92**, 125432 (2015).
176. Asaoka, R., Gea-Banacloche, J., Tokunaga, Y. & Koshino, K. Stimulated emission of superradiant atoms in waveguide quantum electrodynamics. *Phys. Rev. Appl.* **18**, 064006 (2022).
177. McDonnell, C. & Olmos, B. Subradiant edge states in an atom chain with waveguide-mediated hopping. *Quantum* **6**, 805 (2022).
178. Kim, K.-Y. et al. Cavity-mediated collective emission from steady-state subradiance. *Nat. Commun.* **16**, 6346 (2025).
179. van Diepen, C. J. et al. Resonant energy transfer and collectively driven emitters in waveguide QED. *Phys. Rev. Res.* **7**, 033169 (2025).
180. Rattenbacher, D. et al. On-chip interference of scattering from two individual molecules. *Optica* **10**, 1595–1601 (2023).
181. Lange, C. M. et al. Cavity QED with molecular defects coupled to a photonic crystal cavity. Preprint at https://arxiv.org/abs/2506.01917 (2025).
182. Büse, A. et al. Symmetry protection of photonic entanglement in the interaction with a single nanoaperture. *Phys. Rev. Lett.* **121**, 173901 (2018).
183. Maksymov, I. S., Miroshnichenko, A. E. & Kivshar, Y. S. Plasmonic nanoantennas for efficient control of polarization-entangled photon pairs. *Phys. Rev. A* **86**, 011801 (2012).
184. Hou, J., Słowik, K., Lederer, F. & Rockstuhl, C. Dissipation-driven entanglement between qubits mediated by plasmonic nanoantennas. *Phys. Rev. B* **89**, 235413 (2014).
185. Leng, H., Szychowski, B., Daniel, M.-C. & Pelton, M. Strong coupling and induced transparency at room temperature with single quantum dots and gap plasmons. *Nat. Commun.* **9**, 4012 (2018).
186. Cuartero-González, A. & Fernández-Domínguez, A. I. Dipolar and quadrupolar excitons coupled to a nanoparticle-on-mirror cavity. *Phys. Rev. B* **101**, 035403 (2020).
187. Kang, B., Hu, H., Chen, H. & Zhang, Z. Long-range dipole–dipole interactions enabled with the guided plasmons of matched nanoparticle-on-mirror antenna pairs. *Phys. Rev. A* **111**, 013526 (2025).
188. Bedingfield, K., Yuen, B. & Demetriadou, A. Subradiant entanglement in plasmonic nanocavities. *Phys. Rev. B* **111**, 075420 (2025).
189. Boddeti, A. K. et al. Long-range dipole–dipole interactions in a plasmonic lattice. *Nano Lett.* **22**, 22–28 (2022).
190. Boddeti, A. K. et al. Reducing effective system dimensionality with long-range collective dipole–dipole interactions. *Phys. Rev. Lett.* **132**, 173803 (2024).
191. Freire-Fernández, F. et al. Room-temperature polariton lasing from CdSe core-only nanoplatelets. *ACS Nano* **18**, 15177–15184 (2024).
192. Hong, C., Zheng, Z., Patel, S. K. & Odom, T. W. High-chirality polariton lasing from symmetry-broken plasmonic lattices. *ACS Nano* **19**, 18824–18832 (2025).
193. De Giorgi, M. et al. Interaction and coherence of a plasmon–exciton polariton condensate. *ACS Photonics* **5**, 3666–3672 (2018).
194. Ramezani, M. et al. Plasmon-exciton-polariton lasing. *Optica* **4**, 31–37 (2017).
195. Papon, C. et al. Independent operation of two waveguide-integrated quantum emitters. *Phys. Rev. Appl.* **19**, L061003 (2023).
196. Chu, X.-L. et al. Independent electrical control of two quantum dots coupled through a photonic-crystal waveguide. *Phys. Rev. Lett.* **131**, 033606 (2023).
197. Chang, D. E., Vuletić, V. & Lukin, M. D. Quantum nonlinear optics — photon by photon. *Nat. Photon.* **8**, 685–694 (2014).
198. Imamoğlu, A., Schmidt, H., Woods, G. & Deutsch, M. Strongly interacting photons in a nonlinear cavity. *Phys. Rev. Lett.* **79**, 1467–1470 (1997).
199. Lukin, M. D. et al. Dipole blockade and quantum information processing in mesoscopic atomic ensembles. *Phys. Rev. Lett.* **87**, 037901 (2001).
200. Miranowicz, A., Paprzycka, M., Liu, Y.-x, Bajer, J. & Nori, F. Two-photon and three-photon blockades in driven nonlinear systems. *Phys. Rev. A* **87**, 023809 (2013).
201. Kala, A. et al. Opportunities and challenges of solid-state quantum nonlinear optics. *ACS Nano* **19**, 14557–14578 (2025).
202. Gorshkov, A. V., Otterbach, J., Fleischhauer, M., Pohl, T. & Lukin, M. D. Photon-photon interactions via Rydberg blockade. *Phys. Rev. Lett.* **107**, 133602 (2011).
203. Kim, B. et al. A weakly-interacting many-body system of Rydberg polaritons based on electromagnetically induced transparency. *Commun. Phys.* **4**, 101 (2021).
204. Pritchard, J. D. et al. Cooperative atom-light interaction in a blockaded Rydberg ensemble. *Phys. Rev. Lett.* **105**, 193603 (2010).
205. Tiarks, D., Schmidt-Eberle, S., Stolz, T., Rempe, G. & Dürr, S. A photon–photon quantum gate based on Rydberg interactions. *Nat. Phys.* **15**, 124–126 (2019).
206. Stolz, T. et al. Quantum-logic gate between two optical photons with an average efficiency above 40%. *Phys. Rev. X* **12**, 021035 (2022).
207. Peyronel, T. et al. Quantum nonlinear optics with single photons enabled by strongly interacting atoms. *Nature* **488**, 57–60 (2012).
208. Dudin, Y. O. & Kuzmich, A. Strongly interacting Rydberg excitations of a cold atomic gas. *Science* **336**, 887–889 (2012).
209. Firstenberg, O. et al. Attractive photons in a quantum nonlinear medium. *Nature* **502**, 71–75 (2013).
210. Delteil, A. et al. Towards polariton blockade of confined exciton–polaritons. *Nat. Mater.* **18**, 219–222 (2019).
211. Walther, V., Johne, R. & Pohl, T. Giant optical nonlinearities from Rydberg excitons in semiconductor microcavities. *Nat. Commun.* **9**, 1309 (2018).
212. Kazimierczuk, T., Fröhlich, D., Scheel, S., Stolz, H. & Bayer, M. Giant Rydberg excitons in the copper oxide Cu_2O. *Nature* **514**, 343–347 (2014).
213. Lynch, S. A. et al. Rydberg excitons in synthetic cuprous oxide Cu_2O. *Phys. Rev. Mater.* **5**, 084602 (2021).
214. Paul, A. S., Rajendran, S. K., Ziemkiewicz, D., Volz, T. & Ohadi, H. Local tuning of Rydberg exciton energies in nanofabricated Cu_2O pillars. *Commun. Mater.* **5**, 43 (2024).
215. Steinhauer, S. et al. Rydberg excitons in Cu_2O microcrystals grown on a silicon platform. *Commun. Mater.* **1**, 11 (2020).
216. DeLange, J. et al. Highly-excited Rydberg excitons in synthetic thin-film cuprous oxide. *Sci. Rep.* **13**, 16881 (2023).
217. Barua, K. et al. Bottom-up fabrication of 2D Rydberg exciton arrays in cuprous oxide. *Commun. Mater.* **6**, 21 (2025).
218. Gallagher, L. A. P. et al. Microwave-optical coupling via Rydberg excitons in cuprous oxide. *Phys. Rev. Res.* **4**, 013031 (2022).
219. Heckötter, J. et al. Asymmetric Rydberg blockade of giant excitons in cuprous oxide. *Nat. Commun.* **12**, 3556 (2021).
220. Walther, V. & Pohl, T. Plasma-enhanced interaction and optical nonlinearities of Cu_2O Rydberg excitons. *Phys. Rev. Lett.* **125**, 097401 (2020).
221. Morin, C. et al. Self-kerr effect across the yellow Rydberg series of excitons in Cu_2O. *Phys. Rev. Lett.* **129**, 137401 (2022).
222. Makhonin, M. et al. Nonlinear Rydberg exciton-polaritons in Cu_2O microcavities. *Light Sci. Appl.* **13**, 47 (2024).
223. Liu, X. et al. Strong light–matter coupling in two-dimensional atomic crystals. *Nat. Photon.* **9**, 30–34 (2015).
224. Sun, Z. et al. Optical control of room-temperature valley polaritons. *Nat. Photon.* **11**, 491–496 (2017).
225. Zeytinoğlu, S. & İmamoğlu, A. Interaction-induced photon blockade using an atomically thin mirror embedded in a microcavity. *Phys. Rev. A* **98**, 051801 (2018).
226. Walther, V., Zhang, L., Yelin, S. F. & Pohl, T. Nonclassical light from finite-range interactions in a two-dimensional quantum mirror. *Phys. Rev. B* **105**, 075307 (2022).
227. Gu, J. et al. Enhanced nonlinear interaction of polaritons via excitonic Rydberg states in monolayer WSe_2. *Nat. Commun.* **12**, 2269 (2021).
228. Datta, B. et al. Highly nonlinear dipolar exciton-polaritons in bilayer MoS_2. *Nat. Commun.* **13**, 6341 (2022).
229. Zhang, L. et al. Van der Waals heterostructure polaritons with moiré-induced nonlinearity. *Nature* **591**, 61–65 (2021).
230. Takemura, N., Trebaol, S., Wouters, M., Portella-Oberli, M. T. & Deveaud, B. Polaritonic Feshbach resonance. *Nat. Phys.* **10**, 500–504 (2014).
231. Schwartz, I. et al. Electrically tunable Feshbach resonances in twisted bilayer semiconductors. *Science* **374**, 336–340 (2021).
232. Wagner, M. et al. Feshbach resonances in exciton–charge-carrier scattering in semiconductor bilayers. *Phys. Rev. Lett.* **134**, 076903 (2025).
233. Schneider, C., Glazov, M. M., Korn, T., Höfling, S. & Urbaszek, B. Two-dimensional semiconductors in the regime of strong light–matter coupling. *Nat. Commun.* **9**, 2695 (2018).
234. Luo, Y. et al. Strong light–matter coupling in van der Waals materials. *Light Sci. Appl.* **13**, 203 (2024).
235. Hein, M. et al. Entanglement in graph states and its applications. Preprint at https://doi.org/10.48550/arXiv.quant-ph/0602096 (2006).
236. Raussendorf, R. & Briegel, H. J. A one-way quantum computer. *Phys. Rev. Lett.* **86**, 5188 (2001).
237. Browne, D. E. & Rudolph, T. Resource-efficient linear optical quantum computation. *Phys. Rev. Lett.* **95**, 010501 (2005).
238. Zhong, H.-S. et al. 12-photon entanglement and scalable scattershot boson sampling with optimal entangled-photon pairs from parametric down-conversion. *Phys. Rev. Lett.* **121**, 250505 (2018).
239. Walther, P. et al. Experimental one-way quantum computing. *Nature* **434**, 169–176 (2005).
240. Varnava, M., Browne, D. E. & Rudolph, T. How good must single photon sources and detectors be for efficient linear optical quantum computation? *Phys. Rev. Lett.* **100**, 060502 (2008).
241. Pant, M., Krovi, H., Englund, D. & Guha, S. Rate–distance tradeoff and resource costs for all-optical quantum repeaters. *Phys. Rev. A* **95**, 012304 (2017).
242. Thomas, P., Ruscio, L., Morin, O. & Rempe, G. Efficient generation of entangled multiphoton graph states from a single atom. *Nature* **608**, 677–681 (2022).
243. Thomas, P., Ruscio, L., Morin, O. & Rempe, G. Fusion of deterministically generated photonic graph states. *Nature* **629**, 567–572 (2024).

244. Hilaire, P., Vidro, L., Eisenberg, H. S. & Economou, S. E. Near-deterministic hybrid generation of arbitrary photonic graph states using a single quantum emitter and linear optics. *Quantum* **7**, 992 (2023).
245. Lindner, N. H. & Rudolph, T. Proposal for pulsed on-demand sources of photonic cluster state strings. *Phys. Rev. Lett.* **103**, 113602 (2009).
246. Lee, J. et al. A quantum dot as a source of time-bin entangled multi-photon states. *Quantum Sci. Technol.* **4**, 025011 (2019).
247. Economou, S. E., Lindner, N. H. & Rudolph, T. Optically generated 2-dimensional photonic cluster state from coupled quantum dots. *Phys. Rev. Lett.* **105**, 093601 (2010).
248. Gimeno-Segovia, M., Rudolph, T. & Economou, S. E. Deterministic generation of large-scale entangled photonic cluster state from interacting solid state emitters. *Phys. Rev. Lett.* **123**, 070501 (2019).
249. Schwartz, I. et al. Deterministic generation of a cluster state of entangled photons. *Science* **354**, 434–437 (2016).
250. Huet, H. et al. Deterministic and reconfigurable graph state generation with a single solid-state quantum emitter. *Nat. Commun.* **16**, 4337 (2025).
251. Taminiau, T. et al. Detection and control of individual nuclear spins using a weakly coupled electron spin. *Phys. Rev. Lett.* **109**, 137602 (2012).
252. Van der Sar, T. et al. Decoherence-protected quantum gates for a hybrid solid-state spin register. *Nature* **484**, 82–86 (2012).
253. Takou, E., Barnes, E. & Economou, S. E. Precise control of entanglement in multinuclear spin registers coupled to defects. *Phys. Rev. X* **13**, 011004 (2023).
254. Takou, E., Barnes, E. & Economou, S. E. Generation of genuine all-way entanglement in defect-nuclear spin systems through dynamical decoupling sequences. *Quantum* **8**, 1304 (2024).
255. Minnella, J. D., Ouellet, M., Klein, A. R. & Bassett, L. C. Single-gate, multipartite entanglement on a room-temperature quantum register. Preprint at https://doi.org/10.48550/arXiv.2508.08465 (2025).
256. Cramer, J. et al. Repeated quantum error correction on a continuously encoded qubit by real-time feedback. *Nat. Commun.* **7**, 11526 (2016).
257. Widmann, M., Lee, S. Y., Rendler, T. et al. Coherent control of single spins in silicon carbide at room temperature. *Nat. Mater.* **14**, 164–168 (2015).
258. Bourassa, A., Anderson, C. P., Miao, K. C. et al. Entanglement and control of single nuclear spins in isotopically engineered silicon carbide. *Nat. Mater.* **19**, 1319–1325 (2020).
259. Dakis, F., Takou, E., Barnes, E. & Economou, S. E. High-throughput assessment of the controllability of a nuclear-spin register coupled to a defect. *Phys. Rev. Appl.* **22**, 054073 (2024).
260. Bergeron, L. et al. Silicon-integrated telecommunications photon-spin interface. *PRX Quantum* **1**, 020301 (2020).
261. Durand, A. et al. Broad diversity of near-infrared single-photon emitters in silicon. *Phys. Rev. Lett.* **126**, 083602 (2021).
262. Udvarhelyi, P., Somogyi, B., Thiering, G. & Gali, A. Identification of a telecom wavelength single photon emitter in silicon. *Phys. Rev. Lett.* **127**, 196402 (2021).
263. Islam, F. et al. Cavity-enhanced emission from a silicon T center. *Nano Lett.* **24**, 319–325 (2023).
264. Johnston, A., Felix-Rendon, U., Wong, Y.-E. & Chen, S. Cavity-coupled telecom atomic source in silicon. *Nat. Commun.* **15**, 2350 (2024).
265. Redjem, W. et al. All-silicon quantum light source by embedding an atomic emissive center in a nanophotonic cavity. *Nat. Commun.* **14**, 3321 (2023).
266. Saggio, V. et al. Cavity-enhanced single artificial atoms in silicon. *Nat. Commun.* **15**, 5296 (2024).
267. Buterakos, D., Barnes, E. & Economou, S. E. Deterministic generation of all-photonic quantum repeaters from solid-state emitters. *Phys. Rev. X* **7**, 041023 (2017).
268. Li, B., Economou, S. E. & Barnes, E. Photonic resource state generation from a minimal number of quantum emitters. *npj Quantum Inf.* **8**, 11 (2022).
269. Gühne, O., Lu, C.-Y., Gao, W.-B. & Pan, J.-W. Toolbox for entanglement detection and fidelity estimation. *Phys. Rev. A* **76**, 030305 (2007).
270. Tóth, G. & Gühne, O. Entanglement detection in the stabilizer formalism. *Phys. Rev. A* **72**, 022340 (2005).
271. Gühne, O. & Tóth, G. Entanglement detection. *Phys. Rep.* **474**, 1–75 (2009).
272. Knips, L., Schwemmer, C., Klein, N., Wieśniak, M. & Weinfurter, H. Multipartite entanglement detection with minimal effort. *Phys. Rev. Lett.* **117**, 210504 (2016).
273. Tiurev, K. et al. High-fidelity multiphoton-entangled cluster state with solid-state quantum emitters in photonic nanostructures. *Phys. Rev. A* **105**, L030601 (2022).
274. Pallister, S., Linden, N. & Montanaro, A. Optimal verification of entangled states with local measurements. *Phys. Rev. Lett.* **120**, 170502 (2018).
275. Dangniam, N., Han, Y.-G. & Zhu, H. Optimal verification of stabilizer states. *Phys. Rev. Res.* **2**, 043323 (2020).
276. Holland, M. J. & Burnett, K. Interferometric detection of optical phase shifts at the Heisenberg limit. *Phys. Rev. Lett.* **71**, 1355 (1993).
277. Sanders, B. & Milburn, G. Optimal quantum measurements for phase estimation. *Phys. Rev. Lett.* **75**, 2944 (1995).
278. Lee, H., Kok, P. & Dowling, J. P. A quantum Rosetta stone for interferometry. *J. Mod. Opt.* **49**, 2325–2338 (2002).
279. Dowling, J. P. Quantum optical metrology — the lowdown on high-N00N states. *Contemp. Phys.* **49**, 125–143 (2008).
280. Pezze, L., Smerzi, A., Oberthaler, M. K., Schmied, R. & Treutlein, P. Quantum metrology with nonclassical states of atomic ensembles. *Rev. Mod. Phys.* **90**, 035005 (2018).
281. Goban, A. et al. Superradiance for atoms trapped along a photonic crystal waveguide. *Phys. Rev. Lett.* **115**, 063601 (2015).
282. Raussendorf, R., Browne, D. E. & Briegel, H. J. Measurement-based quantum computation on cluster states. *Phys. Rev. A* **68**, 022312 (2003).
283. Bartolucci, S. et al. Fusion-based quantum computation. *Nat. Commun.* **14**, 912 (2023).
284. Bolt, A., Duclos-Cianci, G., Poulin, D. & Stace, T. Foliated quantum error-correcting codes. *Phys. Rev. Lett.* **117**, 070501 (2016).
285. Paesani, S. & Brown, B. J. High-threshold quantum computing by fusing one-dimensional cluster states. *Phys. Rev. Lett.* **131**, 120603 (2023).
286. Song, W., Kang, N., Kim, Y. & Lee, S. Encoded-fusion-based quantum computation for high thresholds with linear optics. *Phys. Rev. Lett.* **133**, 050605 (2024).
287. Azuma, K., Tamaki, K. & Lo, H.-K. All-photonic quantum repeaters. *Nat. Commun.* **6**, 6787 (2015).
288. Borregaard, J. et al. One-way quantum repeater based on near-deterministic photon-emitter interfaces. *Phys. Rev. X* **10**, 021071 (2020).
289. Gerace, D., Laussy, F. & Sanvitto, D. Quantum nonlinearities at the single-particle level. *Nat. Mater.* **18**, 200–201 (2019).
290. Orfanakis, K. et al. Rydberg exciton–polaritons in a Cu_2O microcavity. *Nat. Mater.* **21**, 767–772 (2022).
291. Zhan, Y., Hilaire, P., Barnes, E., Economou, S. E. & Sun, S. Performance analysis of quantum repeaters enabled by deterministically generated photonic graph states. *Quantum* **7**, 924 (2023).
292. Burkard, G., Ladd, T. D., Pan, A., Nichol, J. M. & Petta, J. R. Semiconductor spin qubits. *Rev. Mod. Phys.* **95**, 025003 (2023).
293. Zhang, G., Cheng, Y., Chou, J.-P. & Gali, A. Material platforms for defect qubits and single-photon emitters. *Appl. Phys. Rev.* **7**, 031308 (2020).
294. Azzam, S. I., Parto, K. & Moody, G. Prospects and challenges of quantum emitters in 2D materials. *Appl. Phys. Lett.* **118**, 240502 (2021).
295. Gupta, S., Wu, W., Huang, S. & Yakobson, B. I. Single-photon emission from two-dimensional materials, to a brighter future. *J. Phys. Chem. Lett.* **14**, 3274–3284 (2023).
296. Wang, G. et al. Colloquium: Excitons in atomically thin transition metal dichalcogenides. *Rev. Mod. Phys.* **90**, 021001 (2018).
297. Lehmberg, R. Radiation from an *n*-atom system. I. General formalism. *Phys. Rev. A* **2**, 883 (1970).
298. Lewenstein, M. et al. Ultracold atomic gases in optical lattices: mimicking condensed matter physics and beyond. *Adv. Phys.* **56**, 243–379 (2007).
299. Dutta, O. et al. Non-standard Hubbard models in optical lattices: a review. *Rep. Prog. Phys.* **78**, 066001 (2015).
300. Browaeys, A. & Lahaye, T. Many-body physics with individually controlled Rydberg atoms. *Nat. Phys.* **16**, 132–142 (2020).

Acknowledgements
The authors acknowledge support from the US Department of Energy, Office of Basic Energy Sciences, through the Quantum Photonic Integrated Design Center (QuPIDC) EFRC award DE-SC0025620.

Author contributions
All authors contributed substantially to discussion of the content. L.H. initiated the project. E.D., C.M.L., B.W., A.D., A.S., J. A.M.-L., C., K.B., X.G., Z.Z., V.K.V., S.B., J.M.P., N.L., C.H., J.D.H., V.W., R.T. and L.H. wrote the Review. T.O., M.P., T.L., J.V., V.M.S., A.B. and S.E.E. reviewed and edited the manuscript before submission.

Competing interests
The authors declare no competing interests.

Additional information
Supplementary information The online version contains supplementary material available at https://doi.org/10.1038/s41578-026-00893-8.

Peer review information *Nature Reviews Materials* thanks Adam Gali for their contribution to the peer review of this work.